The Astronomical Journal, 147:137 (16pp), 2014 June doi:10.1088/0004-6256/147/6/137

PARAMETERS AND ABUNDANCES IN LUMINOUS STARS

R. Earle Luck
Department of Astronomy, Case Western Reserve University, 10900 Euclid Avenue, Cleveland, OH 44106-7215, USA; luck@fafnir.astr.cwru.edu
Received 2014 February 20; accepted 2014 March 18; published 2014 May 2

ABSTRACT

Parameters and abundances for 451 stars of spectral types F, G, and K of luminosity classes I and II have been derived. Absolute magnitudes and $E(B-V)$ have been derived for the warmer stars in order to investigate the galactic abundance gradient. The value found here: $d[\mathrm{Fe/H}]/dR \sim -0.06$ dex kpc^{-1}, agrees well with previous determinations. Stellar evolution indicators have also been investigated with the derived C/O ratios indicating that standard CN processing has been operating. Perhaps the most surprising result found in these supposedly relatively young intermediate-mass stars is that both [O/Fe] and [C/Fe] show a correlation with [Fe/H] much the same as found in older populations. While the stars were selected based on luminosity class, there does exist a significant [Fe/H] range in the sample. The likely explanation of this is that there is a significant range in age in the sample; that is, some of the sample are low-mass red-giant stars with types that place them within the selection criteria.

Key words: Galaxy: abundances – stars: abundances – stars: evolution – stars: fundamental parameters

Online-only material: machine-readable and VO tables

1. INTRODUCTION

Abundances of intermediate-mass evolved stars are often used to study the effects of stellar evolution, or as probes of galactic chemical evolution. The stars of interest in this regard are of spectral types F, G, and K and are of luminosity classes I and II. Their masses are 2 $M_\odot$ to upward of 10 $M_\odot$ with total lifetimes of a gigayear or more down to tens of millions of years. These stars have as precursors early F through B main-sequence stars. While on the main sequence, the CN-cycle provides power, and as FGK supergiants, they have passed through the first dredge-up and currently exist as He core-burning objects. The abundances that are of particular interest as indicators of internal evolution are lithium, carbon, nitrogen, and oxygen. The pp-process heavily affects lithium in intermediate-mass stars by destroying the element in about 98% of the star by mass. C, N, and O are involved in CN-cycle energy production and are re-arranged by incomplete CN processing in zones subject to convection to the surface. The expectation is that in stars of this mass and evolutionary phase, lithium will be diluted, carbon will be deficient, nitrogen enhanced, and oxygen constant with respect to the original values. Studies of Li and CNO in supergiants starting with Luck (1978) and extending through Luck & Lambert (2011) have found the expectation borne out in the derived abundances.

In terms of galactic chemical evolution, intermediate-mass evolved stars are of interest as they specify the current level of abundances within the Galaxy. As they are luminous, they can be used to map out the current distribution of elements in the Galactic disk. This second use has been the primary focus of abundance work on these stars in the past 15 yr with Cepheids serving as the probe of choice. The recent studies of Luck et al. (2011) and Luck & Lambert (2011) represent the current state-of-the-art in galactic abundance gradient work based on Cepheid variables. The essential results of these studies are that the galactic metallicity gradient $d[\mathrm{Fe/H}]/dR$ is about -0.055 dex kpc^{-1}, and that there is no evidence for azimuthal variations in abundances.

What can intermediate-mass non-variable evolved stars tell us that Cepheids cannot? First, a large sample of non-variable stars will allow us to study the effects of stellar evolution over a larger range of effective temperatures than Cepheids. This is because Cepheids tend to fall in the effective temperature range 4800–6600 K (Luck et al. 2008) while non-variables can be found at temperatures below and above these limits. Perhaps the main reason to study these stars is to increase the confidence level of the Cepheid gradient work by adding more stars thus covering the sampled area more completely. The number of Cepheids in the latest gradient work (Luck et al. 2011; Luck & Lambert 2011) totals about 450 stars. This is most of the known Type I Cepheids, that is, a Cepheid of Population I with a mass in the range 3–15 $M_\odot$. Non-variable intermediate-mass supergiants have absolute magnitudes comparable to Cepheids and thus probe the same range of distances as Cepheids. Galactic abundance mapping has not used these stars to the same extent as Cepheids because their distances are much more uncertain than are distances for Cepheids. This is due to uncertainties in absolute magnitudes and reddening for the non-variable stars. The intrinsic color calibration of Kovtyukh et al. (2008) and the absolute magnitude calibration of Kovtyukh et al. (2010) ameliorates these problems. It would be profitable to investigate the abundances of non-variables now to see if they can shed further light on the effects of stellar evolution in the mass range of about 2–15 $M_\odot$ as well as fill in data on the galactic metallicity distribution.

Spectroscopic high resolution data has been assembled for 451 stars primarily of spectral type F, G, and K of luminosity classes I and II. The master list for the supergiants (luminosity class I) was assembled using the SIMBAD database. The initial list for the bright giants was the list of Lèbre et al. (2006) supplemented by a search of the *Bright Star Catalog* (Hoffleit & Jaschek 1991). Table 1 gives the list of stars with some basic information. There are a few stars in Table 1 of luminosity class III. These stars are from Lèbre et al. and do meet the criteria for inclusion in this study. It must be emphasized that the selection of intermediate-mass stars by spectral type and luminosity class is far from foolproof. Cepheids provide an example of the problem. Classical Cepheids (aka Type I Cepheids) are intermediate-mass pulsating supergiants of the thin disk, while W Vir stars (aka Type II Cepheids) are low-mass

Table 1
Program Stars

Primary ID	HR	HD	HIP	Type	Spectral Type	Parallax	V	$B-V$	d (pc)	Spectra
HD 725		725	951	Star	F5Ib-II	0.84	7.09	0.58		SE
36 Psc	59	1227	1319	Star	G8II-III	8.00	6.13	0.91	125	SE
HD 1400		1400	1486	Star	K7...	2.92	6.98	1.55	342	E
HD 1457		1457	1526	Star	F0Iab...	-0.10	7.85	0.54		EH
HD 3147		3147	2796	Star	K2Ib-II	1.06	6.96	2.07	943	S
HD 3489		3489	3030	Star	K3Ib-II	0.61	6.79	1.72		S
HD 3588		3588		Star	F1Iab...		8.88	0.63		H
HD 4266		4266	3584	Star	F2Iab...	0.56	6.96	0.37		E
HR 207	207	4362	3649	Star	G0Ib	1.07	6.42	1.04	935	SE
58 Psc	213	4482	3675	Star	G8II	11.52	5.52	0.98	87	SE

Notes. All information except column 11 (Spectra) from SIMBAD. Spectra: Source of spectroscopic material: S is McDonald Observatory Struve Reflector and Sandiford echelle spectrograph. E is Observatoire d'Haute Provence ELODIE spectrograph. H is the Hobbly–Eberly Telescope and High-Resolution Spectrograph. F is the European Southern Observatory/MPG telescope and FEROS spectrograph.

(This table is available in its entirety in machine-readable and Virtual Observatory (VO) forms in the online journal. A portion is shown here for guidance regarding its form and content.)

pulsating supergiants of halo or thick disk origin. Unfortunately, they are difficult to discriminate between either by spectroscopy or photometry. In fact, the major distinguishing characteristic is distance from the galactic plane (Harris 1985). In many cases, it is possible to sort the "odd" stars out only after performing the analysis. This topic will be re-examined in the discussion.

The northern stars were observed using the McDonald Observatory Struve Telescope and Sandiford Cassegrain Echelle Spectrograph and/or the Hobby–Eberly Telescope (HET) and high-resolution spectrograph (HRS). The ELODIE and ESO data archives also provided spectroscopic data for the analysis. The process used for the spectral databases was to obtain a list of all stars available and then retrieve the spectral type for each from SIMBAD. Stars meeting the selection criteria were then processed. The ESO data used was exclusively from the FEROS spectrograph. A number of Cepheid spectra were located in the archival FEROS data that have not been used in gradient analyses by Luck and collaborators. These spectra are included here as a check on methods and results.

2. OBSERVATIONAL MATERIAL

The primary source of observational data for this study is a set of high signal-to-noise ratio (S/N) spectra obtained during numerous observing runs between 1997 and 2010 at McDonald Observatory using the 2.1 m Struve Telescope and the Sandiford Cassegrain Echelle Spectrograph (McCarthy et al. 1993). The spectra continuously cover a wavelength range from about 484 to 700 nm, with a resolving power of about 60,000. Typical S/N values for the spectra are in excess of 150. To enable cancellation of telluric lines, broad-lined B stars were regularly observed with S/N exceeding that of the program stars. The 215 stars observed with the Sandiford spectrograph have an "S" in column 11 of Table 1.

High S/N spectra were obtained during the period 2008 August–2010 November using the HET and its HRS (Tull 1998). These spectra cover a continuous wavelength range from 440 to 785 nm with a resolving power of about 30,000. Typical maximum S/N values (per pixel) for the spectra are in excess of 100. Each night a broad-lined B star with S/N exceeding that of the program stars was observed to enable cancellation of telluric lines. The number of stars observed in this campaign was 92. An "H" in Table 1, column 11, marks these stars.

The ESO Archive was used to obtain Max-Planck-Gesellschaft (MPG) telescope/FEROS spectrograph data on 133 stars including a number of Cepheids not included in Luck et al. (2011). The spectra cover a continuous wavelength range from 400 to 785 nm with a resolving power of about 48,000. Typical maximum S/N values (per pixel) for the spectra are in excess of 150. Broad-lined B stars were located in the archive to enable cancellation of telluric lines. In Table 1, column 11, these stars are marked with an "F."

A further 134 spectra were obtained from the ELODIE Archive (Moultaka et al. 2004). These echelle spectra are fully processed through order co-addition with a continuous wavelength span from about 400 to 680 nm and a resolution of 42,000. Only spectra with S/N $>$ 50 were utilized in this analysis.

The total number of spectra from all sources utilized comes to 574. The greatest overlap is between the Sandiford and ELODIE data with 82 stars in common between these two data sets.

IRAF[1] was used to perform standard CCD processing for the Sandiford, HET, HRS, and FEROS data sets including scattered light subtraction and echelle order extraction. All spectra were extracted using a zero-order (i.e., the mean) normalization of the flat field that removes the blaze from the extracted spectra. A second extraction was done for the HET and FEROS spectra using a high-order polynomial to normalize the flat field. This leaves the blaze function in the extracted spectrum but the spectrum reflects more accurately the true counts along the orders.

A Windows-based graphical package developed by R. Earle Luck (REL) was used to further process the spectra. This included Beer's law removal of telluric lines, smoothing with a fast Fourier transform procedure, continuum normalization, and wavelength setting. Echelle orders show significant S/N variations from edge to maximum due to blaze efficiency. To maximize the S/N in the HET and FEROS spectra we have co-added the order overlap region using as weights the counts from the second data extraction. The co-added spectra were then inspected and the continua sometimes modified by minor

[1] IRAF is distributed by the National Optical Astronomy Observatories, which are operated by the Association of Universities for Research in Astronomy, Inc., under cooperative agreement with the National Science Foundation.

amounts in the overlap regions. Equivalent widths from the spectra were measured using the Gaussian approximation. The line list is a revised one that will be described in the next section.

3. ANALYSIS

3.1. Line List and Analysis Resources

A new line list was created for this study by merging the line list of Kovtyukh & Andrievsky (1999) with the line list of Luck & Heiter (2007). This was supplemented by lines from the unblended solar line lists of Rutten & van der Zalm (1984a, 1984b) along with lines selected from numerous solar abundance analyses. The final line list has 2943 entries. Solar *gf* values were derived from equivalent widths newly measured from the Delbouille et al. (1973) solar intensity atlas. These equivalent widths were done twice (by different measurers) using locally determined continua and direct integration of the line profiles. The double measurement adds a level of assurance over that of a single measurement in that mistakes are more easily recognized and corrected.

To determine *gf* values from the line measures we have adopted the abundances of Asplund et al. (2009) and van der Waals damping coefficients from Barklem et al. (2000) and Barklem & Aspelund-Johansson (2005) or computed using the van der Waals approximation (Unsöld 1938). Hyperfine data for Mn and Co were taken from Kurucz (1992). The solar atmosphere used was from the MARCS model code (Gustafsson et al. 2008).

The derived solar *gf* values for Fe I have been compared to laboratory values taken from the NIST database (Kramida et al. 2013). There are 539 lines in common which show a mean difference in log *gf* in the sense this study minus NIST of -0.012 and a standard deviation (σ) of 0.163. After a 2σ clip the mean difference is -0.008 over 521 lines with a standard deviation of 0.126. Given the good agreement between the solar values and the laboratory values one could ask: why not use laboratory *gf* values in the analysis? The answer is that in the solar list there are 1051 Fe I lines, but that only 539 of those lines are in the laboratory database. The other side is that there are about 500 lines in the laboratory database that are deemed too blended for inclusion in the solar list. A significant increase in the number of reliable laboratory *gf* values is needed, not merely for iron, but for all species.

Comparing the new solar *gf* values to the Kovtyukh & Andrievsky (1999) solar *gf* values a mean difference in log *gf* of -0.041 ($n = 2195$, $\sigma = 0.157$) is found and after a 2σ clip the mean difference is -0.064 ($n = 2112$, $\sigma = 0.100$). A difference is expected due to the differences in technique. Kovytukh & Andrievsky used the solar flux atlas of Kurucz et al. (1984) as the source of their solar spectral material and a solar model computed with ATLAS9 (Kurucz 1992). Given other possible differences in damping constants and partition functions, the agreement we find here is good. Most of the scatter in the values can be attributed to differences in equivalent widths for weak lines (<0.0005 nm) that are sensitive to small continuum variations and profile determination.

Abundances for the bulk of the program stars were calculated using MARCS model atmospheres (Gustafsson et al. 2008). A few of the program stars are hotter than 8000 K and thus outside of the MARCS grids. ATLAS9 models (Kurucz 1992) were computed to determine abundances for these stars. To check abundance consistency between the two model sources a number of stars with effective temperatures down to about 6250 K have been analyzed using both types of models. The line calculations were made using the LINES and MOOG codes (Sneden 1973) as maintained by R. Earle Luck since 1975.

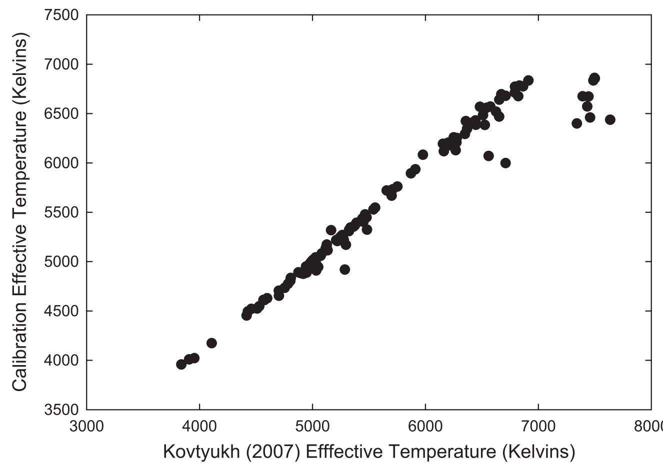

Figure 1. Effective temperatures derived using the Kovtyukh (2007) line ratio–effective temperature calibration vs. the effective temperatures given by Kovtyukh. See the text for discussion.

3.2. Stellar Parameters and Abundances

Initial effective temperatures for the program stars were determined using an updated version of the line-ratio–effective temperature calibration of Kovtyukh (2007). This method is essentially an excitation analysis using ratios of high and low excitation lines calibrated against temperature. An effective temperature determination from a single spectrum is typically based upon 50 or more such line ratios. The individual temperatures from each ratio are averaged and show a standard deviation about the mean temperature of 125 K. Comparison of effective temperatures for stars with multiple spectra shows excellent agreement: the median difference is 13 K. This implies that the continua setting for these stars is very consistent. The temperature determined from the line-ratio calibration serves as the starting effective temperature for the analysis.

Kovtyukh published effective temperatures for 109 of the program stars included here. Figure 1 shows the relation between the Kovtyukh effective temperatures and those found here from the Kovtyukh calibration. Above about 6500 K, there are a number of stars which deviate significantly between the calibration derived temperature and the temperature given by Kovytukh in the sense that the Kovtyukh temperature is much higher. The source of this discrepancy is either in the spectra, or in the current form of the calibration. Many of the spectra used by Kovtyukh are the same as those used here, specifically, the spectra from ELODIE. Additionally, there is no indication among these stars for those that have multiple spectra that there is a significant difference in the temperatures derived from the line-ratio calibration as applied to the separate spectra. One possibility is that updates to the line-ratio calibration have modified the upper temperature range results dramatically. Evidence for this is that the discrepant values encompass all of the common stars with effective temperatures above 7000 K in the Kovtyukh data. This view is reinforced by noting that no calibration relation in the updated version extends beyond 7000 K.

The effective temperatures used in the Kovtyukh calibration were gleaned from a variety of sources including a number of pure excitation analyses. Since the MARCS models of

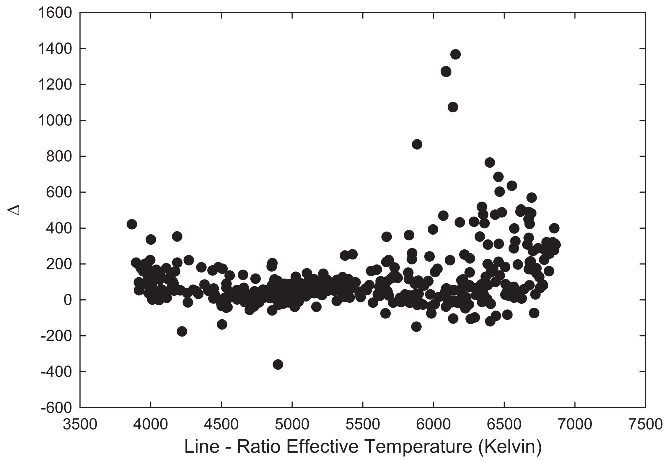

Figure 2. Effective temperatures derived using the Kovtyukh (2007) line-ratio–effective temperature calibration vs. the difference in that temperature and the final MARCS model atmosphere (Gustafsson et al. 2008) derived effective temperature. The sense is MARCS−calibration. MARCS models give somewhat high temperatures across the temperature range and at higher temperatures there is considerable scatter.

Gustafsson et al. (2008) were not used to derive any of the calibrating effective temperatures, it is possible that the line ratio calibration will not yield effective temperatures in precise agreement with what would be needed for a best match to the line data using MARCS models. As a result, the effective temperatures have been revised by examining the excitation data and modifying the effective temperatures to force there to be no dependence of abundance on lower excitation potential for the lines of neutral iron. Most changes are of order +50 to 100 K. However, in a number of cases at temperatures greater than 6500 K, there is significant disagreement between the calibration temperatures and the MARCS derived effective temperatures.

In Figure 2, the difference in adopted and calibration effective temperatures for MARCS models (denoted Δ) is plotted against adopted effective temperature. As can be seen, there is considerable scatter especially toward higher temperatures. The mean difference below 5875 K is +64 K with a standard error of 5 K. At higher temperatures, the line-ratio method has increasing difficulties with weakening neutral lines, making noise and continuum issues more prevalent. Another problem is the applicability of the calibration. A case in point in Figure 2 is the star at an effective temperature of 5895 K and a Δ of 890 K. This star is HD 56126, better known as IRAS 07140–2321. It has a spectral type of F5 Iab and is a well-known post-AGB object with abundance anomalies (Rao et al. 2012). Other peculiar objects in the analysis will be discussed briefly later.

The effective temperature calibration of Kovtyukh (2007) cuts off at an effective temperature of around 7000 K and above 6800 K the temperatures are suspect. Above this temperature, an excitation analysis of either neutral (below 7500 K) or once ionized iron was used to set the temperature. For the stars above 8000 K, the most recent version of the PASTEL database (Soubiran et al. 2010) was consulted for an appropriate effective temperature, and Fe II was then used to refine the value chosen.

The photospheric acceleration due to gravity, commonly called the gravity (g), and given as log g where g is in cgs units, was determined using an ionization balance. This involves forcing the neutral and ionized species of iron to give the same total abundance using the gravity as the free parameter. The microturbulent velocity was determined by forcing the abundance given by the lines of neutral iron to show no dependence on line strength. These two forcing operations are performed simultaneously with the excitation analysis. This process starts by interpolating a set of three models at appropriate gravities at the starting effective temperature from the MARCS grid (Gustafsson et al. 2008). The iron line data is then run through each model at a series of microturbulent velocities. These operations are monitored through an interactive iron-editing program that allows the deletion of outliers that can have undue influence on the various relations. Improved parameters are calculated after each calculation set. In general, the improved parameter set found after the initial run matches the data very well. Parameter confirmation is done by interpolating a new model at the proper parameters. This model is then used to recompute the iron data relations and confirm the excitation and ionization balance along with the lack of dependence of iron abundance on line strength.

These stars exhibit a range of metallicities and this is taken into account as the parameter determination proceeds. Below [Fe/H] of −0.3, models with [M/H] = −0.5 are used, from [Fe/H] of −0.3 to +0.15 solar metallicity models are employed, and above [Fe/H] = +0.15 models with [M/H] = +0.25 are utilized. The preferred models are 5 $M_\odot$, no α enhancement, moderate CN processing, and 2 km s^{-1} Doppler velocity. There is little effect on the abundances due to a change from 5 to 2 $M_\odot$ or from a change of 2 to 5 km s^{-1}, so if a preferred model is not available, a change in grid is made. The only region where models are severely lacking is above 6750 K at gravities below log g of 1.5. As indicated before, this is the region where ATLAS models have been implemented in the analysis.

Adopted parameters are given in Table 2 for both MARCS and ATLAS models. In some cases, parameters could not be rectified between the various spectra. This is not unexpected as many of these stars are variables. In these cases, multiple entries can be found in the parameter table for the star in question. Average abundances for 27 elements with $Z > 10$ are in Table 3 and Li and CNO abundances are presented in Table 4 on a per spectrum basis. The data in Table 3 and 4 are on a per spectrum basis; for example, if a star has both an ELODIE and a Sandiford spectrum then abundances determined from each are given separately. Details of the abundances (per species average, σ, and number of lines) are available upon request.

3.3. Li, C, N, and O Analysis

For lithium, carbon, nitrogen, and oxygen, spectrum syntheses for the features of interest have been performed utilizing laboratory oscillator strengths where available. For the lithium feature, all components of ^{7}Li (using the data presented by Andersen et al. 1984) in the 670.7 nm hyperfine doublet were used to match the observed profiles. There is no evidence in the observed spectra for the presence of ^{6}Li and therefore, it was not considered in the syntheses. Lithium abundance data are presented in Table 4 and in Figure 3 matches to several stars are shown.

Carbon abundances have been derived from C I lines at 505.2 nm, 538.0 nm, and 711.5 nm and the C_2 Swan system lines at 513.5 nm. Note that neither the Sandiford or ELODIE spectra extend to 711.5 nm. For the atomic lines, the oscillator strengths of Biémont et al. (1993) or Hibbert et al. (1993) were adopted. These oscillator strengths have been used in determinations of the solar carbon abundance (Asplund et al. 2005). For the Swan C_2 syntheses, $f(0, 0) = 0.0303$ (Grevesse et al. 1991) was adopted with the relative band f values of Danylewych & Nicholls (1974), along with $D_0 = 6.210$ eV

Table 2
Parameters and [Fe/H]

Primary ID	Tag	Type	T (K)	log(g) (cm s^{-2})	V_t (km s^{-1})	[Fe/H]
			MARCS Models			
HD 725	hd000725	Star	6856	1.62	2.81	0.02
36 Psc	hr0059	Star	5041	2.82	1.37	0.15
36 Psc	hd001227	Star	5066	2.55	1.34	0.20
HD 1400	hd001400	Star	4107	0.73	1.84	−0.31
HD 1457	hd001457	Star	6910	1.00	2.50	−0.24
HD 3147	hd003147	Star	4113	1.11	2.90	0.19
HD 3489	hd003489	Star	4266	1.35	2.67	0.07
HR 207	hr0207	Star	5423	1.62	3.34	0.09
58 Psc	hr0213	Star	4989	2.87	1.28	0.25
zet And	hr0215	EllipVar	5064	2.88	3.58	−0.05

Notes. Tag: identifier used in subsequent tables to allow discrimination between stars with multiple parameter sets. The tag in some cases provides an alternate identification for the object.

(This table is available in its entirety in machine-readable and Virtual Observatory (VO) forms in the online journal. A portion is shown here for guidance regarding its form and content.)

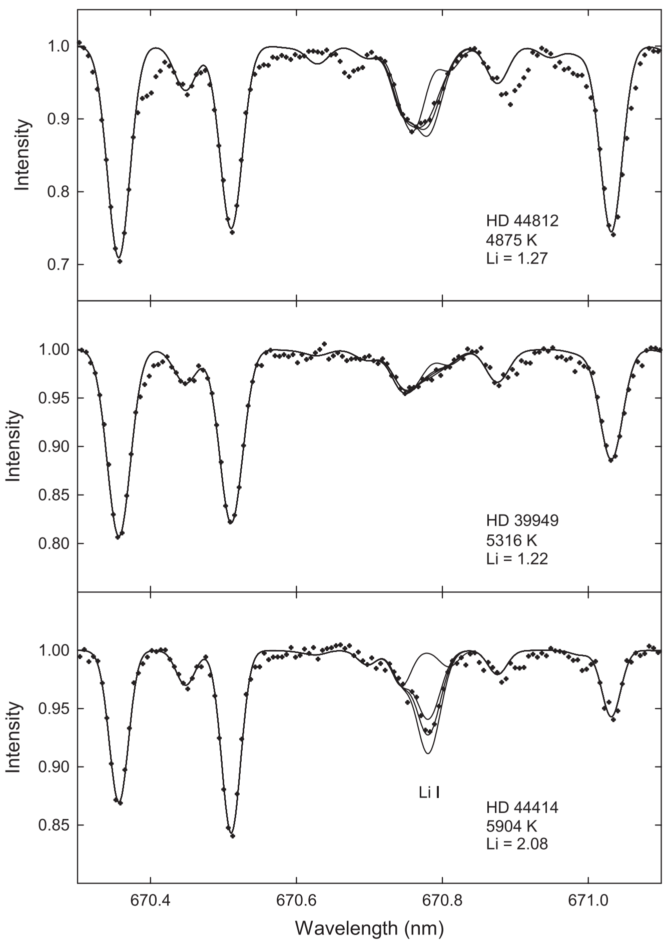

Figure 3. Syntheses of Li I at 670.7 nm in three stars of varying temperature showing a range of Li strengths. The abundance given in each panel is the best-fit abundance. Panels with multiple syntheses are at three abundances that indicate the best-fit abundance ±0.1 dex.

(Grevesse et al. 1991) and theoretical line wavelengths (as needed) from C. Amiot (1982, private communication). To form the carbon abundance on a per spectrum basis the individual features are combined as follows: for $T_{\rm eff} < 5000$ K, 538.0 has weight 1 while 513.5 has weight 3. At $T > 5000$ K, 505.2, 513.5, and 711.5 have weight 1 while 538.0 has weight 2. The weights are based on relative strength and blending. Typical spreads in abundance for the features are 0.15 dex. For the purpose of abundances with respect to solar values, we adopt log $\varepsilon_{\rm C} = 8.45$, very close to the Asplund et al. (2009) recommended solar carbon abundance of 8.43. Table 4 has the average CNO data on a per star (or phase) basis. If more than one spectrum is available for a star, the abundances from each are combined as simple means. In Figure 4 several representative fits to C I 538.0 nm are shown.

Nitrogen abundances are derived only for stars having FEROS or HET spectra using the N I lines at 744.2 and 746.8 nm. Oscillator strengths for these lines were taken from the inverted solar analysis of Kovtyukh & Andrievsky (1999). The nitrogen abundance was determined using a grid of syntheses to determine the best fit to the two lines. Note that these lines are only usable in stars with effective temperatures greater than 5500 K. To determine nitrogen abundances relative to the Sun we use log $\varepsilon_{\rm N} = 7.99$—the Grevesse et al. (1996) solar nitrogen abundance used to compute the oscillator strengths. These abundances are in Table 4.

Oxygen abundance indicators in the available spectral range are rather limited: the O I triplet at 615.6 nm and the [O I] lines at 630.0 and 636.3 nm. The O I triplet at 777.5 nm is heavily affected by non-LTE effects and thus not usable in a standard LTE analysis. The O I 615.8 lines are problematic in abundance analyses with only the 615.8 nm line being retained in solar oxygen analyses (Asplund et al. 2004). The O I lines were synthesized using the NIST atomic parameters (Kramida et al. 2013) that were also used by Asplund et al. For the forbidden oxygen lines only 630.0 nm is usable as 636.3 nm is weak, heavily blended, and complicated by the presence of the Ca I autoionization feature. In the syntheses of 630.0 nm, the line data presented by Allende et al. (2001) was used except that the experimental oscillator strength for the blending Ni I line (Johansson et al. 2003) was adopted. The syntheses assumed [Ni/Fe] = 0. To form a final oxygen abundance the data was average in the following manner: for $T_{\rm eff} < 5500$ K only [O I] is used, while for $T_{\rm eff} > 5500$ K, O I has weight 1 and [O I] has weight 2. At an effective temperature of 6400 K, [O I] is essentially not detectable and the abundance depends only on O I 615.8 nm. For $T_{\rm eff} < 5500$ K the C–O dependence has been

Table 3
Abundances for the Program Stars

Tag	S	Na	Mg	Al	Si	S	Ca	Sc	Ti	V	Cr	Mn	Fe	Co	Ni	Cu	Zn	Rb	Sr	Y	Zr	Ba	La	Ce	Nd	Sm	Eu
MARCS Models																											
104aqr	S	0.54	0.24	0.42	0.26	0.13	0.18	0.36	0.29	0.16	0.24	0.18	0.19	0.20	0.11	−0.02	0.23		1.44	0.31	0.20		0.53	0.40	0.34	−0.13	0.31
12peg	S	0.39		0.91	0.55	0.87	0.48	−0.10	0.05	0.16	0.41	0.19	0.15	0.14	0.13					−0.18	−0.08		0.80	0.36	0.32	0.46	0.45
12peg	E	0.37		0.92	0.53	1.67	0.59	0.10	0.03	0.17	0.43	0.17	0.13	0.30	0.25		−0.04			−0.15	−0.28		0.87	0.47	0.32	0.60	0.33
32cyg	S	0.86	−0.04	0.37	0.50	1.80	0.20	−0.18	0.05	0.16	0.28	0.07	−0.03	0.20	0.07				0.30	−0.01	−0.30		0.26	0.25	0.29	1.00	0.19
32cyg	E	0.85	−0.05	0.40	0.52	1.78	0.04	−0.20	0.06	0.11	0.29	−0.08	−0.10	0.14	0.08		−0.52		0.38	−0.08	−0.08		0.07	0.37	0.14	0.41	0.16
3cet	S		0.35	0.21	0.52	2.04	0.23	−0.06	0.04	0.07	0.32	0.06	0.14	0.22	0.16				0.18	−0.12	−0.39		0.29	0.23	0.25	0.48	0.12
3cet	E		0.24	0.18	0.51	1.95	0.29	−0.10	0.02	0.06	0.32	0.00	0.03	0.18	0.18		−0.35		0.18	−0.20	−0.24		0.22	0.27	0.23	0.07	0.32
45dra	S	0.25	−0.11	0.19	0.04	0.01	−0.08	0.31	0.03	0.00	0.11	−0.14	−0.08	−0.04	−0.13	−0.40	−0.09		0.91	0.20	0.44		0.19	0.18	0.16	−0.36	0.16
45dra	E	0.31	−0.01	0.13	0.07	0.04	−0.02	0.25	0.04	0.02	0.09	−0.13	−0.11	0.12	−0.07	−0.35	−0.26		0.87	0.38	0.42		0.21	0.36	0.18	0.15	0.15
47cyg	S		0.40	0.09	0.49	2.05	0.19	−0.01	0.11	0.27	0.39	−0.11	0.13	0.19	0.25				0.39	0.05	−0.13		0.51	0.48	0.55	0.70	0.62

Note. S, source of spectra (see Table 1).

(This table is available in its entirety in machine-readable and Virtual Observatory (VO) forms in the online journal. A portion is shown here for guidance regarding its form and content.)

Table 4
Average Li, C, N, and O Abundances

Tag	T (K)	log(g) (cm s^{-2})	V (km s^{-1})	[Fe/H]	Li	Type	C	N	O	[C/H]	[N/H]	[O/H]	[C/Fe]	[N/Fe]	[O/Fe]
							MARCS Models								
104aqr	5680	2.52	2.81	0.19	1.03	L	8.04		8.88	−0.41		0.19	−0.60		−0.01
12peg	4482	1.24	3.44	0.14	0.65	L	8.02		8.50	−0.43		−0.19	−0.57		−0.33
32cyg	4106	0.52	2.61	−0.07	0.78	A	8.02		8.50	−0.43		−0.19	−0.37		−0.12
3cet	4152	0.90	3.26	0.08	−0.15	L	8.24		8.72	−0.21		0.03	−0.30		−0.05
45dra	6157	1.78	3.93	−0.10	1.04	L	8.11		8.70	−0.34		0.01	−0.24		0.11
47cyg	4217	1.23	3.89	0.13	−0.27	L	8.11		8.85	−0.34		0.16	−0.47		0.03
56peg	4539	1.76	1.99	−0.05	0.42	L	8.26		8.65	−0.19		−0.04	−0.14		0.01
63cyg	4204	1.27	2.53	0.12	−0.28	L	8.26		8.91	−0.19		0.22	−0.31		0.10
9peg	4931	1.91	2.81	0.13	1.46	A	8.17		8.78	−0.28		0.09	−0.41		−0.04
ahvela	6102	1.66	3.27	0.09	1.46	L	8.07	8.38	8.70	−0.38	0.39	0.01	−0.47	0.31	−0.08

Note. Type: A, abundance; L, abundance upper limit; Li, C, N, and O: log abundance of species with respect to H = 12.

(This table is available in its entirety in machine-readable and Virtual Observatory (VO) forms in the online journal. A portion is shown here for guidance regarding its form and content.)

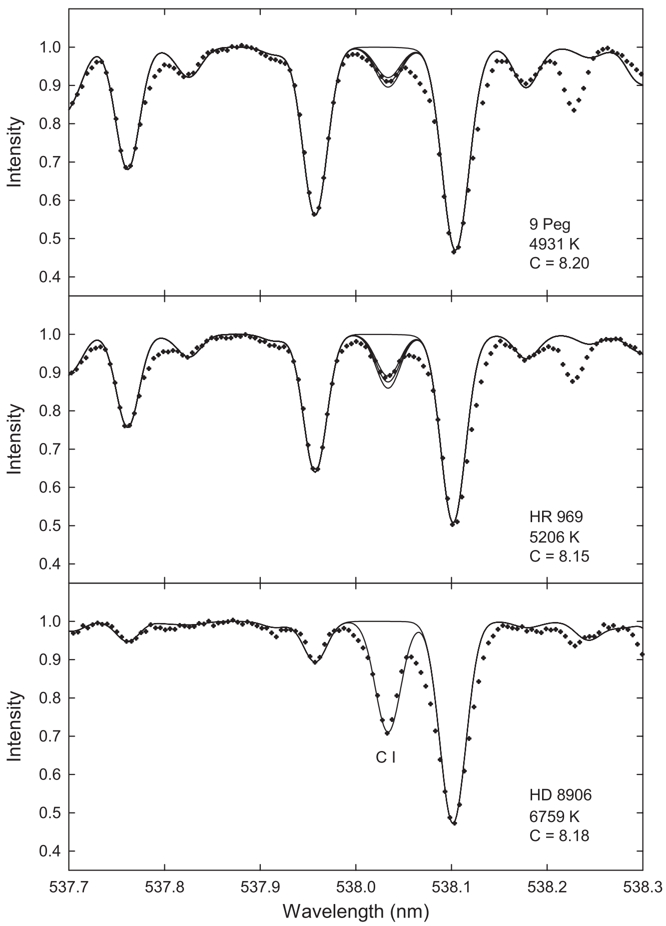

Figure 4. Syntheses of C I 538.0 nm in three stars of varying temperature. The abundance given in each panel is the best-fit abundance. Panels with multiple syntheses are at three abundances that indicate the best-fit abundance ±0.1 dex.

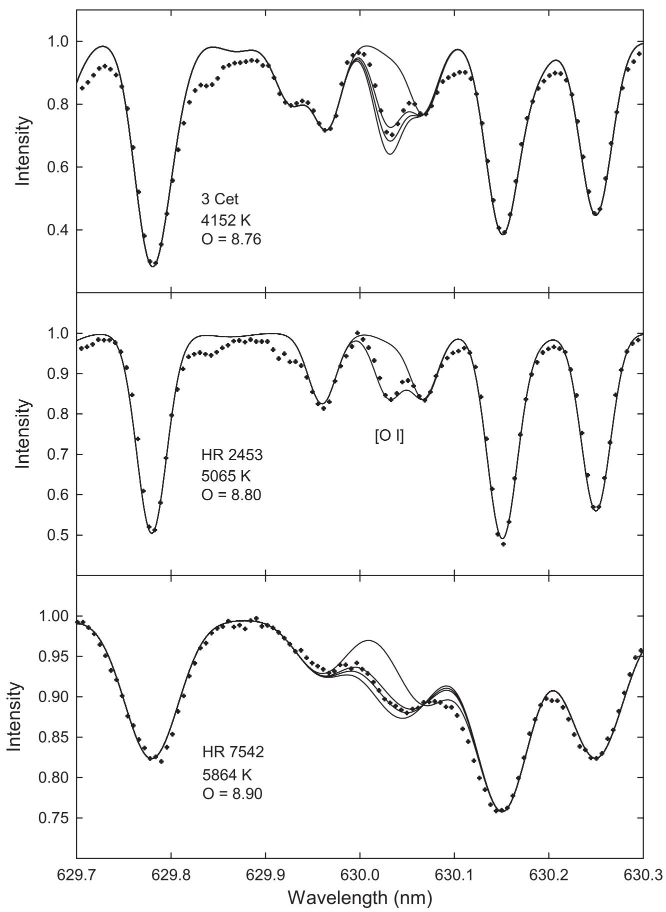

Figure 5. Syntheses of [O I] 630.0 nm in three stars of varying temperature. The abundance given in each panel is the best-fit abundance. Panels with multiple syntheses are at three abundances that indicate the best-fit abundance ±0.1 dex.

explicitly taken into account. Mean oxygen abundance from the individual analyses can be found in Table 4. Figure 5 shows the [O I] line in several stars while Figure 6 shows the quality of fit achievable for the O I 615.8 triplet.

3.4. Departures from Thermodynamic Equilibrium

In dealing with luminous stars, one always worries about possible departures from LTE affecting the excitation and ionization level populations. Luck & Lambert (2011) discussed these problems for Cepheids. Since the 2011 discussion there have been considerations of non-LTE effects in oxygen by Luck et al. (2013) and in barium by Andrievsky et al. (2013, 2014), but the overall comments of Luck & Lambert relevant to non-LTE effects in intermediate-mass stars remain current. Their general conclusion was that while the effects of non-LTE appear to be small for most elements, their presence remains a possibility

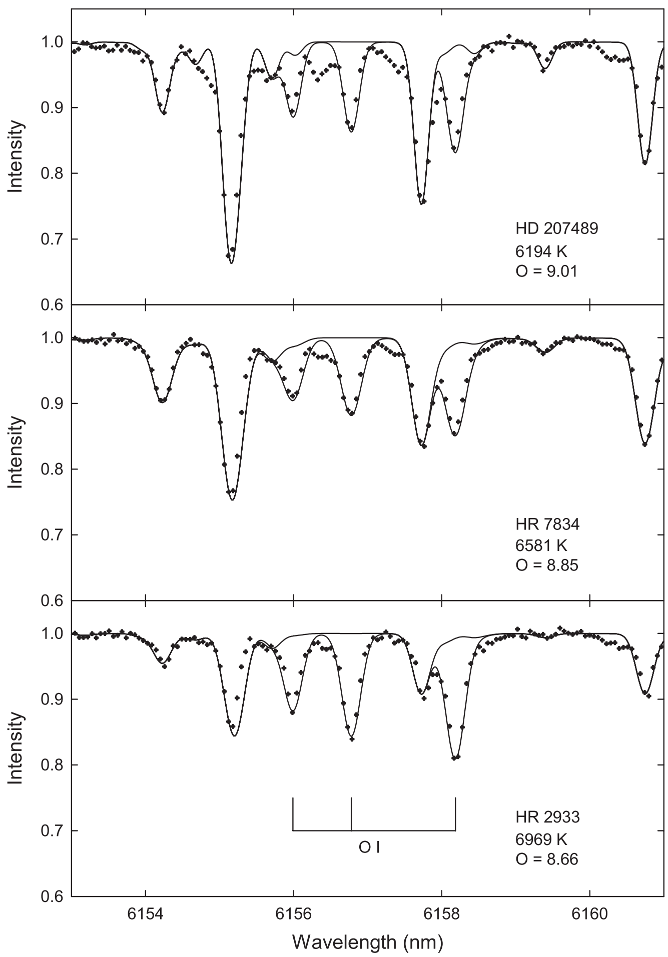

Figure 6. Syntheses of O I 615.8 nm in three hotter stars. The abundance given in each panel is the best-fit abundance.

and that the possibility of non-LTE perturbing the results must be kept in mind in the consideration of elemental abundances.

3.5. Abundance and Parameter Comparisons

To locate previous analyses of our program stars the PASTEL database (Soubiran et al. 2010) was consulted. Over 240 of the program stars have data in PASTEL. The total number of references generated is in excess of 100 for the extant analyses; however, more than 70 of these references contain only one or two stars in common with this work. The author with the largest number of references for previous analyses is the author of this paper. To investigate the parameter and abundance comparison, a subset of the available data has been selected. Trends in temperature and gravity have been sought but only random variations or constant offsets found. The selected studies are discussed below.

For the first comparison, previous analyses of Luck and coworkers were retrieved from PASTEL. These analyses span a period of 30 yr and involve a variety of techniques including effective temperatures from photometry and from excitation analyses, gravities from masses as well as ionization balances, and an evolving set of atomic data. There is corresponding data on a total of 96 stars some of which are Cepheids that do not allow parameter comparisons. Nevertheless, the mean differences relative to this study are astonishingly small: +11 K in temperature ($\sigma = 189$, $n = 72$), +0.05 in log g ($\sigma = 0.51$), and -0.05 in [Fe/H] ($\sigma = 0.19$, $n = 96$). The standard deviation about the means indicates substantial scatter, but no more than found relative to other, more coherent sets of comparison analyses. However, as one might expect there are serious discrepancies in the data. The most obvious case is for HR 8752 (V509 Cas)—a G0 Ia–O supergiant. Since the star is variable, parameter comparison is moot, but [Fe/H] values can be compared. Luck (1975) and Fry & Aller (1975) obtained a [Fe/H] ratio of +0.03 and +0.10, respectively, while the value determined here is -0.74! The reliability of an abundance analysis of a star such as HR 8752 is very poor.

Lyubimkov et al. (2010) have performed an analysis of 42 stars in common with the MARCS analyses of this work. The common stars are mostly F and G supergiants. There is a mean offset of +99 K in the effective temperatures, -0.01 in log g, and +0.08 in [Fe/H]. While not provided in the PASTEL database, the microturbulent velocities derived in Lyubmikov et al. have been compared to the values derived here. The mean microturbulent velocity found by Lyubmikov et al. for the common stars is 3.47 km s^{-1} versus 2.95 km s^{-1} determined here. This difference in microturbulence will translate to an abundance difference of about +0.07 with this study yielding the larger values. This is very close to the difference noted. The overall agreement between the two studies is acceptable.

Another source of comparison is the study by McWilliam (1990). The 31 common stars in this case are mostly G and K bright giants. The effective temperatures show a mean difference of +53 K while the gravities differ in the mean by -0.32 dex. The temperature agreement is good especially considering the McWilliam determination is from photometry while this study uses an excitation analysis. The gravity determination method used by McWilliam was a physical determination using masses derived from luminosities and effective temperatures whereas this study uses a spectroscopic method, i.e., an ionization balance. Spectroscopic and physical determinations of gravities are known to show systematic differences (see Luck & Heiter 2007 for examples) and this appears to be yet another case. To put the McWilliam gravities on the scale of this study, a factor of two decrease in mass would be needed which is perhaps not coincidentally the same as needed to rectify the McWilliam gravity scale with the physical scale of Luck & Heiter (2007). The mean difference in [Fe/H] is +0.25 with this study having the larger values. The parameter differences noted between the studies cannot explain the difference in [Fe/H]. The temperature difference is too small to offset the abundances significantly and the gravity difference is in the wrong sense. However, a comparison of the microturbulent velocities used in the two studies does yield a possible cause. The subset of stars in the comparison has a mean microturbulent velocity of 3 km s^{-1} in the McWilliam study while here the mean velocity is 2 km s^{-1}. All other things being equal, this difference in microturbulence will lead to abundances about 0.25 dex higher in this study as observed.

Hekker & Meléndez (2007) performed a traditional spectroscopic parameter determination; i.e., an excitation and ionization balance, on 15 of the stars considered here. The mean offsets in effective temperature, gravity, and [Fe/H] are: 53 K ($\sigma = 107$), -0.22 dex ($\sigma = 0.36$), and +0.24 dex ($\sigma = 0.12$) respectively. The number of lines used by Hekker & Meléndez was 20 Fe I lines and 6 Fe II lines versus the 350–400 Fe I lines and 20–40 Fe II lines used here. A comparison of the *gf* values between the two studies shows good agreement: a mean difference in log *gf* of -0.02 for Fe I and a difference of +0.01 for

Fe II in the sense Hekker & Meléndez minus the work. There is considerable scatter in the gravities but this is expected given the small number of Fe II lines used to set that value in Hekker & Meléndez. Examination of the microturbulent velocities yields the result that the Hekker & Meléndez values average about 0.3 km s^{-1} higher than the values found here. This translates to an expected abundance offset of +0.08 in the sense that the abundances here should be higher. This only partially explains the difference in [Fe/H] noted. Another likely contributor lies in the model atmospheres used in the respective analyses—MARCS (2008) used here versus Kurucz (1992) in Hekker & Meléndez.

Within this study are a number of Cepheids considered by Sziládi et al. (2007). This study uses the same FEROS spectra as Sziládi et al., allowing direct comparison of the results. Sziládi et al. used a small set of Fe I and Fe II lines, 77 and 18 lines respectively, to perform an excitation and ionization analysis to set the stellar parameters. The microturbulent velocity was determined by demanding there be no dependence of iron abundance on equivalent width. The mean offsets for effective temperature, log g, and [Fe/H] are 9 K ($\sigma = 185$), 0.05 dex ($\sigma = 0.46$), and 0.15 dex ($\sigma = 13$) based on 32 comparisons. The mean effective temperatures and gravities are in good agreement. The scatter is large most likely because Sziládi et al. assigned the Cepheid temperatures and gravities to model grid points spaced at increments of 250 K and 0.5 dex, respectively. The difference in [Fe/H] is at least partially due to the difference in microturbulent velocities: the Sziládi et al. values average 4.2 km s^{-1}, which is 1 km s^{-1} higher than the values found here. The expected [Fe/H] difference is about +0.06 dex with this study having the higher values. A likely source of the microturbulent velocity mismatch in this case is residual temperature effects in the iron data due to setting the effective temperatures and gravities to model grid points.

The analysis of Lèbre et al. (2006) of 145 bright giants provides 59 stars in common with this study. This large overlap is intentional as the Lèbre et al. star list formed a basic framework for the class II stars considered here. The overarching purpose of the Lèbre et al. study was to determine lithium abundances for their sample. To do this they adopted literature effective temperatures or determined the temperature from the $B-V$ color. They do not derive gravities or microturbulent velocities for their stars, instead adopting log $g = 2.0$ and $V_t = 2.0$ km s^{-1} for the bulk of their sample. A comparison of their adopted temperatures with those determined here shows an average offset of +61 K (σ = 248 K) and a median offset of −3 K. The scatter in the temperature differences is significant. Three cases typify the overall problem. The temperature quoted by Lèbre et al. for HR 3102 (HD 65228) is 5600 K while Luck & Wepfer (1995) give 5900 K and the value determined here is 5868 K. As a zeroth order check on the temperatures, consider the observed $B-V$ color of 0.686 as taken from SIMBAD. The Lèbre et al. temperature of 5600 K implies an intrinsic color of 0.727 according to the $B-V$ model calibration of Castelli (1999) at a gravity of 2.0 dex. While the Castelli calibration may not be the best available, the difficulty is well illustrated: the inferred intrinsic color is redder than the observed color! At 5900 K, the intrinsic $B-V$ is about 0.62–0.64 (from Castelli 1999 and Kovtyukh et al. 2008 respectively) which leads to a modest reddening of 0.07 mag or less. As similar problem exists for HR 7449. The observed $B-V$ for the star is 1.05. The effective temperature determined here is 4849 K versus 4210 K given by Lèbre et al. Following the same tack as above,

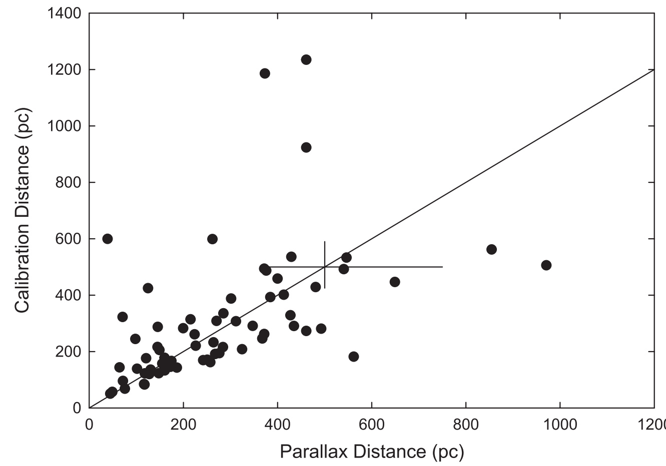

Figure 7. Distances derived from *Hipparcos* parallaxes (van Leeuwen 2007) vs. distances derived from the Kovtyukh et al. (2008, 2010) color and absolute magnitude calibrations. The error bars are for parallax error equal to 1/3 parallax, and for a combined distance modulus uncertainty of 0.36 mag.

the Lèbre et al. temperature implies an interstellar "bluing" of about 0.3 mag. For the temperature determined here, the $B-V$ observed and intrinsic colors are consistent. As a last specific example, HR 3613 shows very discrepant temperatures. The Lèbre et al. temperature is 4800 K while the temperature determined here is 4468 K. It appears that the Lèbre et al. temperature was taken from McWilliam (1990). There are two other temperature determinations in the literature, 4380 K from Hekker & Meléndez (2007) and 4610 K from di Benedetto (1998). Looking once again at the $B-V$ color the observed color is too blue for the Hekker & Meléndez temperature. Using the Lèbre et al./McWilliam temperature the implied color excess in $B-V$ is about 0.15 mag. However, the Hakkila et al. (1997) reddening map says HR 3613 should be unreddened. The parameters determined here are consistent with little to no reddening for HR 3613. As a last point concerning Lèbre et al., they claim that a partial reason for the differences in lithium abundances noted between their study and Luck & Wepfer (1995) is that Luck & Wepfer used inaccurate v sin i and/or macroturbulences in their syntheses. Their evidence for this is the literature values quoted in Table 1 of Luck & Wepfer. However, Luck & Wepfer made detailed fits of the line profiles and gave the actual broadening values used in the syntheses in Table 4 and demonstrated the quality of the fits in Figures 4–7. Further examples of the quality of the synthetic spectra fits can be found in Figures 3–6 here.

As a last external comparison, the stellar parameters and [M/H] ratios determined from FEROS spectra by the AMBRE project (Worley et al. 2012) are considered. There are 26 objects in common with this study. The basic procedure used in the AMBRE project is a fitting process against a library of synthetic spectra generated using MARCS models (Gustafsson et al. 2008). The mean difference (this work − AMBRE) for effective temperature is −76 K (σ = 216), for log g the difference is −0.03 dex (σ = 0.70), and for metallicity (interpreted as [Fe/H] for this work) the difference is +0.27 (σ = 0.22). The means appear acceptable but the scatter is very large in both the temperatures and gravities: the range in differences for temperature is −273 to +439 K while the range in the difference in gravity is −1.97 to +1.52. Given the scatter in parameters, it is very difficult to assess the quality of the metallicities.

Table 5
Distance Information

ID	Tag	Type	l	b	A_v	M_v	$d1$	$d2$	$d3$	d	R_G
104 Aqr	104aqr	∗in∗∗	59.40	−71.44	0.29	−1.51		162	257	162	8.24
12 Peg	12peg	Star	76.64	−22.83					427	427	8.19
V1488 Cyg	32cyg	EB∗Algol	83.67	7.05					325	325	8.24
3 Cet	3cet	V∗	87.07	−70.04					641	641	8.26
d Dra	45dra	Star	86.20	24.99	0.26	−3.73		446	649	446	8.25
56 Peg	56peg	Star	95.12	−31.71	0.21				181	181	8.29
63 Cyg	63cyg	∗in∗∗	88.88	0.20					316	316	8.27
9 Peg	9peg	V∗	71.98	−26.51	0.30	−2.62		215	284	215	8.21
V474 Per	9per	PulsV∗∼	135.51	−4.79	0.96				1000	1000	9.01
AH Vel	ahvel	deltaCep	262.44	−6.96			580		752	580	8.37

Notes. l and b, galactic latitude and longitude respectively. A_v computed from intrinsic color calibration of Kovtyukh et al. (2008) and observed color. M_V computed using the calibration of Kovtyukh et al. (2010). $d1$ is the heliocentric distance in parsecs taken from Luck & Lambert (2011) or computed in the same manner. $d2$ is the heliocentric distance computed from A_V and M_V. $d3$ is the heliocentric distance from the parallax. d is the adopted heliocentric distance. R_G is the galactocentric distance in kiloparsecs computed assuming the solar galactocentric distance to be 8.28 kpc (Schönrich 2012).

(This table is available in its entirety in machine-readable and Virtual Observatory (VO) forms in the online journal. A portion is shown here for guidance regarding its form and content.)

The MARCS grid (Gustafsson et al. 2008) does not extend to temperatures above 8000 K and at higher grid temperatures there is a lack of lower gravity models. As a result, ATLAS9 models (Kurucz 1992) with the Castelli (1996) convection modification were used in the analyses. To check on consistency the analysis was extended down to effective temperatures around 6250 K. The number of stars with both ATLAS and MARCS analyses is 95. The line-data selection for both is identical. The mean differences in effective temperate, gravity, microturbulence, and [Fe/H] are 30 K ($\sigma = 74$), −0.04 dex ($\sigma = 0.26$), 0.04 km s^{-1} ($\sigma = 0.18$), and −0.07 dex ($\sigma = 0.07$), respectively, in the sense MARCS minus ATLAS. Ten of the stars have parameters in the MARCS analysis at the edge of the model grid. If these are eliminated the means do not change significantly but the standard deviations about the mean drop by about a factor of two. The exception is for [Fe/H] for which the mean and standard deviation are little affected by the elimination of these ten stars. The [Fe/H] difference indicates a systematic offset between abundances computed using the different model sources, as parameter changes of the size noted will not cause a difference in computed abundance in either type of model. Luck & Lambert (2011) also noted this difference. As the MARCS analyses are by far the larger group, those analyses will form the basis for further discussion.

3.6. Distances

Distances for the program stars are available through one or more of the following: parallax, the Cepheid PL, or by spectroscopic calibrations yielding $E(B-V)$ and M_V. In Table 5, distance information including galactic latitude and longitude is given for the 350 stars that at least one of these possibilities gives a distance. The parallax data comes from *Hipparcos* and here the values as given by the SIMBAD database (van Leeuwen 2007) are used. Only parallax values greater than three times the error are retained. For the purposes of galactic abundance gradient work, the currently available parallax data is of limited value as it only samples a very limited range of distances around the solar neighborhood. Cepheid distances are taken from Luck & Lambert (2011) or are determined in an analogous manner.

To determine the remaining distances the calibrations of Kovtyukh et al. (2008, 2010) are used. The line-of-sight extinction is determined from the intrinsic $B-V$ color as determined from the Kovtyukh et al. (2008) relation, the observed color as taken from SIMBAD, and $R_V = 3.2$. The intrinsic color calibration uses the stellar parameters and [Fe/H] data. The calibration stars extend down to 4500 K. If one attempts to determine intrinsic $B-V$ values below this temperature the result most often is a negative reddening value. The absolute magnitude M_V is found using the line-ratio calibration of Kovtyukh et al. (2010). This calibration extends over an effective temperature range of 4900–7000 K. This effectively means that most of the K stars in this work do not have distances. Figure 7 shows the parallax-derived distances against the calibration distances. While the overall scales appear commensurate, there is considerable scatter that rises with increasing distance. The error bars shown at 500 pc assume the parallax error is 1/3 the parallax. The calibration error bar assumes a total uncertainty in the distance modulus of 0.36 mag. The latter error stems from the quadrature addition of the quoted uncertainty in the M_V calibration of ±0.2 mag and in $E(B-V)$ of 0.1 mag. The bulk of the scatter appears to be related to the uncertainty in the observed parallaxes. To convert to the distances to galactocentric radii, the solar system is assumed to be at 8.27 kpc from the galactic center (Schönrich 2012).

4. DISCUSSION

4.1. The Galactic Abundance Gradient

One of the major impetuses for this analysis was to use the composition of these stars to determine the galactic abundance gradient. Two of the elements most commonly used for this purpose are iron and oxygen. In Figures 8 and 9 the [Fe/H] and [O/H] ratios are shown as a function of galactocentric radius (R_G). Figure 10 shows the abundance ratio [O/Fe] versus R_G. The essential result of these figures is that the gradient determination is dominated by the Cepheids and luminous stars with distances determined from the Kovtyukh et al. (2008, 2010) color and absolute magnitude calibrations. The parallax stars are within 1 kpc of the solar system, both in actual distance and R_G, and thus contribute little to the gradient determination. What is apparent about the very local stars is that they show much more dispersion in abundance than do the more distant stars. This is

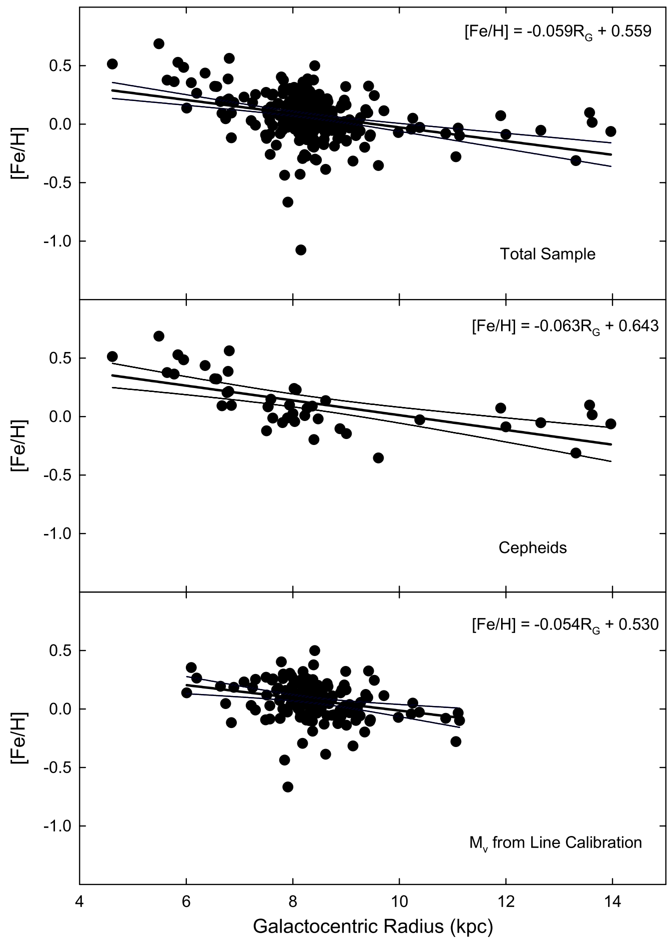

Figure 8. Galactic abundance gradient as determined from [Fe/H]. The top panel shows the complete sample, the middle panel only Cepheids, and the bottom panel only the stars with distances determined from the Kovtyukh et al. (2008, 2010) color and absolute magnitude calibrations. The solar galactocentric distance is 8.27 kpc. The data in all cases is consistent with a gradient of $d[\mathrm{Fe/H}]/dR \approx -0.06$ dex kpc^{-1}. The 95% confidence band is shown for each relation.

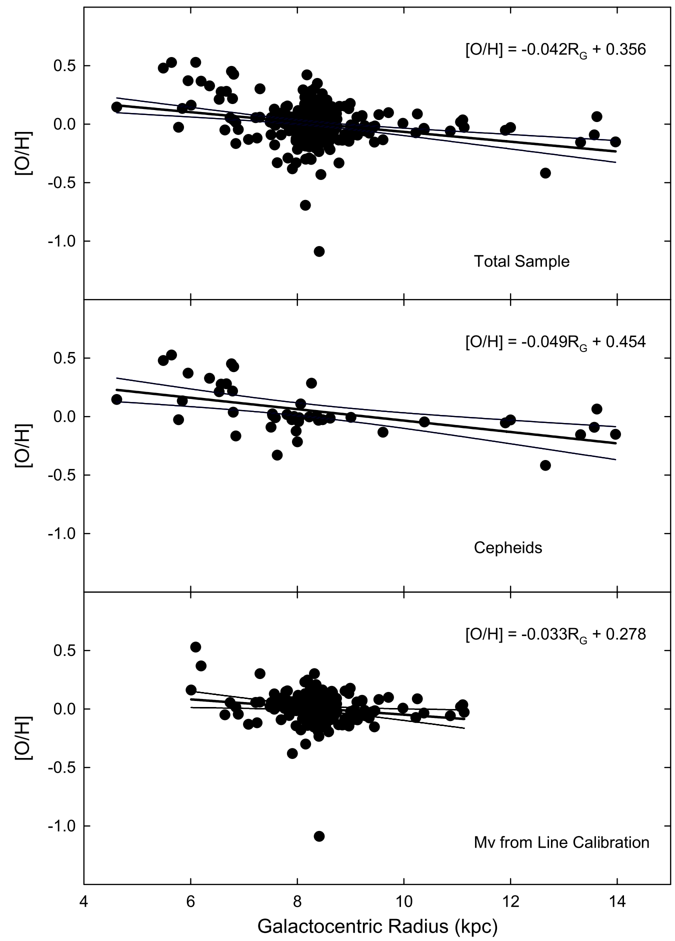

Figure 9. Galactic abundance gradient as determined from [O/H]. The top panel shows the complete sample, the middle panel only Cepheids, and the bottom panel only the stars with distances determined from the Kovtyukh et al. (2008, 2010) color and absolute magnitude calibrations. The data in all cases is consistent with a gradient of $d[\mathrm{O/H}]/dR \approx -0.04$ dex kpc^{-1}. The 95% confidence band is shown for each relation.

because the local stars are an admixture of types while the distant stars are more coherent in their characteristics with Cepheids and non-variable supergiants of type F and G dominating the distant stars. All stars selected for this work have luminosity classes of I or II but the class II stars mainly fall within 1 kpc of the Sun and are a much more heterogeneous in their properties than are classical Cepheids. This highlights one of the primary problems in selecting stars for gradient work—selecting stars based on spectral type and luminosity class admits a wide variety of stars. This problem will be addressed briefly in the next section.

The gradients exhibited in Figures 8–10 are consistent with previous determinations of the galactic abundance gradient. Luck & Lambert (2011) from a sample of 313 Cepheids derived a gradient $d[\mathrm{Fe/H}]/dR_{\mathrm{G}} = -0.061 \pm 0.003$ dex kpc^{-1}. The value found here is $\approx -0.06 \pm 0.01$ with the precise value depending on the subsample used. For $d[\mathrm{O/H}]/dR_{\mathrm{G}}$ and $d[\mathrm{O/Fe}]/dR_{\mathrm{G}}$, Luck & Lambert found -0.056 ± 0.003 and 0.005 ± 0.007, respectively. The values found here are about -0.04 ± 0.01 and 0.01 ± 0.01. The agreement is good considering the difference in sample consistency and the length of baseline.

The total number of elements with determined abundances in this study is 29. In Table 6 gradient data for each species is given in the form $d[\mathrm{x/H}]/dR_{\mathrm{G}}$ and $d[\mathrm{x/Fe}]/dR_{\mathrm{G}}$. Iron which has been determined from hundreds of lines that were subjected to substantial scrutiny, and oxygen, determined from detailed fits to [O I], are the most reliable gradients. The remaining gradients that are reliable are those determined from many ($n > 10$) lines. These species include Si, Ca, and Ni. The gradients for these species range from -0.05 to -0.07 in $d[\mathrm{x/H}]/dR_{\mathrm{G}}$ and essentially have zero slope in $d[\mathrm{x/Fe}]/dR_{\mathrm{G}}$. The abundance from yttrium was determined from five to ten lines and the resulting gradient $d[\mathrm{Y/H}]/dR_{\mathrm{G}}$ is about -0.04 with essentially no gradient in $d[\mathrm{Y/Fe}]/dR_{\mathrm{G}}$. These results are consistent with the results of Luck & Lambert (2011) who provide numerous plots of their gradient data.

Andrievsky et al. (2013, 2014) find in essence no gradient in barium. However, this is at odds with the results for barium found here and is at odds with the s/r elements from this and other studies. The caveat for barium is that the Ba II lines used in the Andriesky et al. work (and here) are very strong lines and are thus very susceptible to line-formation effects in model atmospheres; that is, they are formed near the outer edge of the atmosphere and may not be adequately modeled. Additionally, abundances derived from strong lines are exceedingly sensitive to the microturbulent velocity. As a result, barium gradients in all cases are suspect.

Table 6
Gradients: Species = $a^*R_G + b$

	Total Sample						Cepheid						Mv From Line Calibration					
	Gradient		Uncertainty				Gradient		Uncertainty				Gradient		Uncertainty			
Species	a	b	a	b	σ	N	a	b	a	b	σ	N	a	b	a	b	σ	N
[C/H]	−0.024	−0.141	0.035	0.297	0.662	335	−0.065	0.292	0.011	0.094	0.169	44	0.081	−1.100	0.089	0.748	0.913	164
[C/Fe]	0.035	−0.699	0.035	0.294	0.655	335	−0.002	−0.352	0.010	0.082	0.148	44	0.136	−1.631	0.088	0.742	0.905	164
[N/H]	−0.002	0.301	0.023	0.201	0.365	91	−0.051	0.643	0.017	0.145	0.222	35	0.130	−0.792	0.044	0.381	0.361	48
[N/Fe]	0.052	−0.234	0.025	0.210	0.381	91	−0.003	0.151	0.013	0.114	0.174	35	0.201	−1.462	0.046	0.399	0.378	48
[O/H]	−0.042	0.356	0.008	0.070	0.155	335	−0.049	0.454	0.011	0.099	0.177	44	−0.033	0.279	0.014	0.118	0.144	164
[O/Fe]	0.016	−0.202	0.010	0.080	0.179	335	0.014	−0.190	0.011	0.095	0.170	44	0.022	−0.253	0.019	0.157	0.191	164
[Na/H]	−0.059	0.939	0.013	0.110	0.243	329	−0.078	1.161	0.014	0.123	0.215	44	−0.035	0.753	0.019	0.160	0.195	163
[Na/Fe]	−0.004	0.411	0.010	0.084	0.184	329	−0.020	0.567	0.009	0.080	0.140	44	0.020	0.217	0.015	0.122	0.149	163
[Mg/H]	−0.072	0.784	0.011	0.095	0.213	332	−0.079	0.972	0.014	0.122	0.219	45	−0.056	0.634	0.020	0.164	0.200	163
[Mg/Fe]	−0.012	0.221	0.010	0.080	0.177	332	−0.016	0.329	0.010	0.085	0.153	45	0.000	0.092	0.018	0.151	0.184	163
[Al/H]	−0.059	0.767	0.011	0.094	0.209	334	−0.056	0.791	0.015	0.129	0.231	45	−0.071	0.858	0.018	0.153	0.187	163
[Al/Fe]	−0.001	0.210	0.008	0.065	0.144	334	0.008	0.148	0.008	0.070	0.125	45	−0.017	0.332	0.013	0.106	0.129	163
[Si/H]	−0.053	0.704	0.009	0.075	0.167	337	−0.059	0.745	0.010	0.086	0.155	45	−0.043	0.586	0.012	0.103	0.125	164
[Si/Fe]	0.006	0.145	0.007	0.060	0.134	337	0.004	0.102	0.004	0.035	0.063	45	0.011	0.055	0.009	0.076	0.093	164
[S/H]	−0.096	1.307	0.028	0.231	0.516	337	−0.093	1.071	0.020	0.175	0.314	45	−0.113	1.236	0.027	0.227	0.277	164
[S/Fe]	−0.038	0.748	0.027	0.226	0.504	337	−0.030	0.428	0.015	0.125	0.224	45	−0.059	0.705	0.022	0.189	0.231	164
[Ca/H]	−0.052	0.575	0.009	0.079	0.176	337	−0.053	0.658	0.013	0.110	0.197	45	−0.055	0.589	0.015	0.125	0.152	164
[Ca/Fe]	0.007	0.015	0.006	0.047	0.105	337	0.010	0.015	0.007	0.056	0.101	45	0.000	0.058	0.008	0.071	0.086	164
[Sc/H]	0.002	0.131	0.018	0.155	0.256	277	−0.010	0.457	0.032	0.295	0.321	22	−0.029	0.474	0.022	0.185	0.203	138
[Sc/Fe]	0.046	−0.283	0.015	0.124	0.205	277	0.028	0.043	0.019	0.173	0.188	22	0.034	−0.116	0.021	0.178	0.195	138
[Ti/H]	−0.033	0.444	0.011	0.089	0.198	337	−0.036	0.572	0.015	0.129	0.232	45	−0.025	0.409	0.015	0.130	0.159	164
[Ti/Fe]	0.026	−0.115	0.008	0.071	0.158	337	0.027	−0.071	0.010	0.083	0.150	45	0.030	−0.122	0.014	0.118	0.144	164
[V/H]	−0.021	0.345	0.012	0.098	0.217	337	−0.031	0.452	0.012	0.106	0.191	45	0.007	0.118	0.019	0.156	0.191	164
[V/Fe]	0.038	−0.215	0.011	0.089	0.198	337	0.032	−0.191	0.008	0.067	0.120	45	0.061	−0.413	0.019	0.162	0.198	164
[Cr/H]	−0.040	0.537	0.009	0.077	0.172	337	−0.041	0.527	0.011	0.097	0.174	45	−0.038	0.534	0.014	0.114	0.139	164
[Cr/Fe]	0.019	−0.023	0.007	0.058	0.129	337	0.022	−0.116	0.007	0.062	0.111	45	0.017	0.003	0.011	0.090	0.110	164
[Mn/H]	−0.067	0.731	0.012	0.100	0.223	337	−0.072	0.758	0.012	0.105	0.188	45	−0.063	0.671	0.017	0.147	0.179	164
[Mn/Fe]	−0.008	0.172	0.009	0.073	0.163	337	−0.009	0.115	0.008	0.071	0.127	45	−0.008	0.140	0.011	0.089	0.109	164
[Fe/H]	−0.059	0.559	0.009	0.076	0.168	337	−0.063	0.643	0.012	0.102	0.182	45	−0.055	0.531	0.015	0.124	0.151	164
[Fe/Fe]	−0.059	0.559	0.009	0.076	0.168	337	−0.063	0.643	0.012	0.102	0.182	45	−0.055	0.531	0.015	0.124	0.151	164
[Co/H]	−0.002	0.225	0.012	0.104	0.231	337	−0.020	0.359	0.015	0.130	0.234	45	0.037	−0.111	0.018	0.155	0.189	164
[Co/Fe]	0.057	−0.334	0.012	0.102	0.228	337	0.043	−0.284	0.011	0.096	0.172	45	0.092	−0.642	0.022	0.188	0.230	164
[Ni/H]	−0.054	0.553	0.010	0.081	0.181	337	−0.048	0.547	0.011	0.098	0.176	45	−0.072	0.701	0.016	0.138	0.169	164
[Ni/Fe]	0.005	−0.007	0.006	0.050	0.111	337	0.015	−0.096	0.007	0.063	0.113	45	−0.018	0.170	0.011	0.090	0.110	164
[Cu/H]	−0.060	0.626	0.020	0.172	0.383	316	−0.066	0.556	0.016	0.140	0.251	45	−0.046	0.378	0.026	0.222	0.270	163
[Cu/Fe]	−0.001	0.057	0.019	0.159	0.353	316	−0.003	−0.087	0.010	0.087	0.155	45	0.011	−0.180	0.021	0.178	0.217	163
[Zn/H]	−0.099	0.956	0.023	0.196	0.419	314	−0.105	0.872	0.018	0.157	0.265	40	−0.094	0.843	0.029	0.244	0.290	161
[Zn/Fe]	−0.047	0.454	0.021	0.180	0.385	314	−0.051	0.315	0.013	0.114	0.192	40	−0.040	0.310	0.024	0.203	0.241	161
[Rb/H]	−0.062	0.534	0.031	0.257	0.374	62	−0.099	0.763	0.036	0.299	0.390	20	0.096	−0.850	0.050	0.415	0.255	26
[Rb/Fe]	0.001	−0.093	0.028	0.230	0.335	62	−0.029	0.099	0.031	0.256	0.333	20	0.134	−1.291	0.039	0.321	0.197	26
[Sr/H]	0.108	−0.287	0.048	0.402	0.483	222	−0.011	0.814	0.053	0.470	0.331	14	0.161	−0.583	0.063	0.534	0.472	105
[Sr/Fe]	0.166	−0.814	0.049	0.416	0.500	222	0.042	0.316	0.057	0.506	0.356	14	0.238	−1.288	0.068	0.577	0.510	105
[Y/H]	−0.039	0.625	0.021	0.172	0.337	320	−0.041	0.818	0.031	0.264	0.397	36	−0.039	0.685	0.032	0.267	0.316	158
[Y/Fe]	0.017	0.100	0.019	0.157	0.308	320	0.023	0.181	0.031	0.266	0.399	36	0.011	0.199	0.031	0.260	0.307	158
[Zr/H]	0.015	0.148	0.020	0.172	0.383	337	−0.001	0.399	0.018	0.151	0.270	45	0.049	−0.023	0.030	0.254	0.310	164
[Zr/Fe]	0.073	−0.411	0.020	0.168	0.374	337	0.062	−0.244	0.013	0.116	0.208	45	0.104	−0.554	0.034	0.288	0.351	164
[Ba/H]	−0.021	0.459	0.026	0.217	0.365	186	0.003	0.370	0.016	0.131	0.182	24	−0.083	1.078	0.053	0.448	0.405	76
[Ba/Fe]	0.049	−0.181	0.021	0.178	0.300	186	0.084	−0.419	0.021	0.167	0.232	24	−0.040	0.650	0.041	0.349	0.315	76
[La/H]	0.007	0.281	0.019	0.159	0.272	290	0.038	−0.040	0.030	0.269	0.301	26	−0.033	0.601	0.026	0.215	0.252	147
[La/Fe]	0.048	−0.120	0.015	0.130	0.222	290	0.073	−0.403	0.023	0.206	0.230	26	0.024	0.052	0.023	0.190	0.222	147
[Ce/H]	−0.015	0.433	0.014	0.119	0.266	336	0.006	0.278	0.016	0.135	0.243	45	−0.064	0.821	0.024	0.199	0.243	164
[Ce/Fe]	0.044	−0.126	0.012	0.104	0.232	336	0.069	−0.365	0.011	0.094	0.168	45	−0.009	0.290	0.022	0.184	0.224	164
[Nd/H]	−0.008	0.318	0.013	0.110	0.246	336	0.009	0.137	0.016	0.135	0.242	45	−0.052	0.657	0.023	0.192	0.235	164
[Nd/Fe]	0.050	−0.240	0.011	0.095	0.212	336	0.072	−0.507	0.012	0.104	0.187	45	0.003	0.126	0.020	0.171	0.209	164
[Sm/H]	−0.028	0.469	0.021	0.173	0.387	336	0.003	0.154	0.013	0.113	0.203	45	−0.101	0.967	0.036	0.300	0.367	164
[Sm/Fe]	0.031	−0.091	0.020	0.171	0.382	336	0.066	−0.490	0.009	0.076	0.137	45	−0.046	0.436	0.036	0.300	0.366	164
[Eu/H]	−0.012	0.297	0.014	0.116	0.258	333	−0.004	0.210	0.016	0.134	0.241	44	−0.033	0.483	0.023	0.190	0.232	163
[Eu/Fe]	0.047	−0.258	0.012	0.098	0.219	333	0.059	−0.433	0.012	0.106	0.191	44	0.022	−0.047	0.020	0.171	0.208	163

Note. σ is the standard deviation of the fit using N stars.

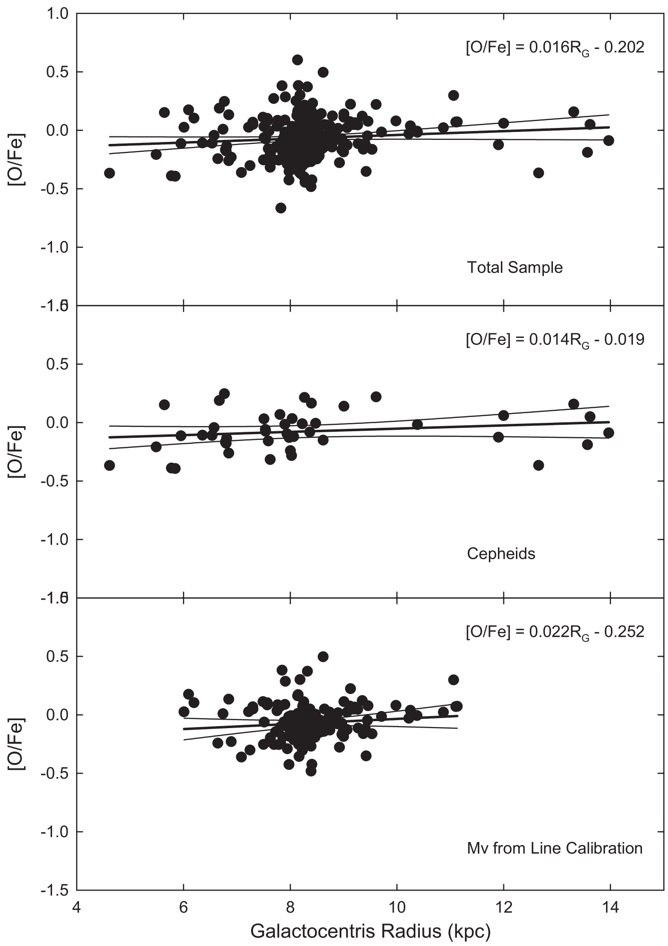

Figure 10. Galactic abundance gradient as determined from [O/Fe]. The top panel shows the complete sample, the middle panel only Cepheids, and the bottom panel only the stars with distances determined from the Kovtyukh et al. (2008, 2010) color and absolute magnitude calibrations. The data in all cases is consistent with no gradient in d[O/Fe]/dR. The 95% confidence band is shown for each relation.

The possibility of a change in the slope of the metallicity gradient at $R_G \sim 7.5$ to 8 kpc is also apparent in Figure 8. Andrievsky et al. (2002) first addressed this, but larger samples such as that of Luck & Lambert (2011) do not show this effect to the extent seen here or in Andrievsky et al. It remains to be proven if the uptick is real or not.

Abundance gradients of the observed magnitude are consistent with chemical evolution models such as those of Cescutti et al. (2007). The inference from the gradient data is that element building up to the time of formation of the latest generation of intermediate-mass stars leads to different absolute yields as a function of galactocentric radius, i.e., $d[\mathrm{x/H}]/dR_G < 0$, but that the ratio of elements built does not depend upon position, that is, $d[\mathrm{x/Fe}]/dR_G < 0 = 0$. One might wonder if the Milky Way shows azimuthal variations in abundance at constant radii. While this study does not have sufficient data to investigate this proposition, the studies of Luck et al. (2011) and Luck & Lambert (2011) address this problem and find no azimuthal variation. This means that the Galaxy is azimuthally well mixed and that it mixes on relatively short timescales.

A primary purpose of this work was to determine if later-type stars other than Cepheids could yield reliable data for a gradient determination. It appears that this is the case; nevertheless, Cepheids still appear to be the better choice for reliable gradient determination. As Luck & Lambert and Luck et al. (2011) provided an extensive discussion of the observational properties of the gradient, the reader is referred to those papers for more details concerning the distribution of the elements in the current Milky Way disk.

4.2. Sample Selection

The common view of F/G/K supergiants is that they are the evolved counterparts of main-sequence A through O stars with masses of 3 to upward of 20 solar masses. Selecting F/G/K supergiants for gradient work might seem fairly objective; however, consider the case of HR 5880. The spectral type is G0Iab:pe and except for the "pe" it might appear to be an excellent candidate. HR 5880 is better known as R CrB, and is most definitely not a normal star. It is a large amplitude variable and a carbon star. Another case is TY Vir, a G3Ibpv star. The spectral type and luminosity class look appropriate; however, it is a metal-poor semi-regular variable most likely belonging to the halo population. They have been analyzed in this work as a check on methods. For R CrB, the temperature and gravity are consistent with previous work, but the [Fe/H] ratio determined here is very high. For TY Vir, the parameters and abundances match previous work quoted in PASTEL very nicely. Another star of interest is HD 121261, a G2/G3II star whose spectrum was found in the archival FEROS data. The parameters are consistent with a supergiant—an effective temperature of 4457 K and a gravity of 0 dex. However, the [Fe/H] value is −1.6. This star is a metal-poor red giant first identified by Bond (1980). Lastly, there is HD 56126 (CY CMi), an F5 Iab supergiant. It is a well-known post-AGB carbon star. The gradient Figures 8–10 do not include these stars as they lack distances.

Included in the gradient figures are s Her (HR 6152), LN Hya (HR 4912), HR Lib (HR 5930), and V1452 Aql. The first three stars are the metal-poor stars in Figure 8 near the solar galactocentric radius. They have little influence on the gradient determination as the large number of stars near the solar radius overwhelms them. HR 6152 is a G8II star taken from the Lèbre et al. (2006) list of bright giants. The parameters found here are consistent with it being a cool supergiant. However, it has an [Fe/H] ratio of −1.08, and is thus a red giant of either the thick disk or halo. Luck et al. (1983) first pointed out HR 4912 as a peculiar metal-poor supergiant. Later work has shown that it is related to the post-AGB stars and/or high latitude supergiants (Rao et al. 2012). HR 5930 has a spectral type of A2 Ib/II and is either a δ Sct (GCVS) or a λ Boo star. The parameters and abundances derived here agree very well with those of North et al. (1994) and ignoring the chemical peculiarities, imply a metal-poor F dwarf. V1452 Aql is supposedly a low-amplitude Cepheid (CEP: - GCVS). The parameters were set by a traditional excitation and ionization analysis with the result an effective temperature of 8045 K and a gravity of 2.84 dex. This is somewhat hot for a Cepheid but the unusual thing is that the derived [Fe/H] ratio is +0.8! To lower the [Fe/H] to solar the temperature would need to drop to about 7000 K. Another oddity is that V1452 Aql has a measurable lithium line. It is not clear where or if there is a problem with this star.

Another problem with object selection is the "simple" problem of spectral type or luminosity class error. The luminosity class is the larger problem in a study of type. Two stars that illustrate this are TYC 1583-944-1 and ALS 11459. They have spectral types of FIab:p and G0Ib, respectively. Their temperatures are consistent with the spectral types but the gravities are log $g = 3.5$–3.6. This would be more consistent with a giant classification, perhaps even an F dwarf, or more likely, a star

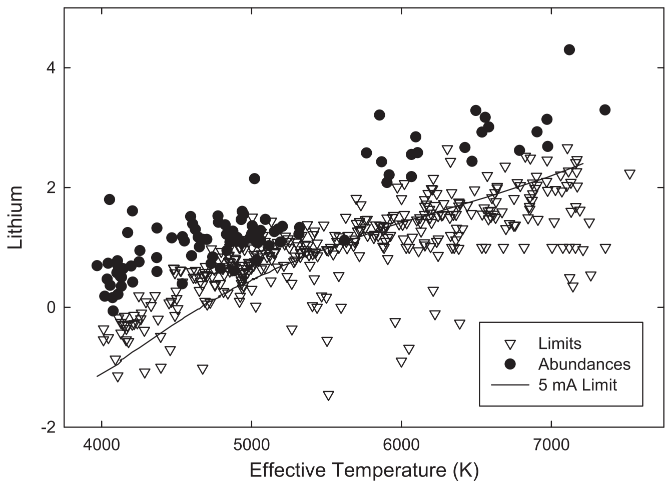

Figure 11. Lithium abundances and abundance limits vs. effective temperature for the program stars. See Section 4.3.1 for a discussion.

near the main-sequence turn-off. The latter is implied by the fact that they both have observable lithium features with abundances at about 2.3—very close to what is found in F dwarfs and turn-off stars. (Lambert & Reddy 2004; Luck & Heiter 2006; Lèbre et al. 2006). Unfortunately, while this discussion might appear exhaustive, there is little doubt that other pathological, or at least disconcerting, cases exist in this sample.

4.3. Li, CNO in Luminous Stars

4.3.1. Lithium

Lithium abundances in FGK luminous stars are characterized by severe dilutions with respect to their original values (Iben 1966a). Standard stellar evolution predicts a dilution of a factor of about 60. The difficulty is that in the progenitor B stars only about the outer 2% by mass of the star retains any lithium after the main sequence. This makes the lithium abundance after the first giant branch very sensitive to mass-loss prior to the onset of convective mixing. Assuming an initial abundance of 3.0 dex (with respect to H = 12), FGK supergiants and bright giants should show lithium abundances of about 1.2 dex or less. In Figure 11 the lithium abundances or limits derived using the MARCS models are shown as a function of the effective temperature. The stars with effective temperatures below 5500 K are consistent with the theoretical expectations in the sense that the abundances (or limits) are, on the whole, at Li = 1.2 dex or less. There is a hint that as the temperatures decline that the lithium abundances also decline. This could imply that the convective mixing in the cooler stars is somewhat deeper, leading to larger amounts of dilution, but this is far from certain.

Of greater interest in Figure 11 are the stars at 6000 K and above that have lithium abundances very close to the assumed initial abundance of Li = 3.0 dex. The star with the highest abundance of lithium is R CrB and it is not of interest in the context of this study. The remaining stars appear to be a bonanza of new super-Li stars. However, this is unlikely to be the case as inspection of the stellar parameters for the high abundance Li stars shows that they have gravities most often around 3.5 dex. This gravity is the expected value for 1.7 $M_\odot$ stars in 6000–7000 K effective temperature range somewhere between the main sequence and the turn-off (Schaller et al. 1992). This means that the lithium content has not been diluted by the first dredge-up. The carbon and nitrogen abundances are also affected by the first dredge-up. Comparison of the carbon and nitrogen abundances for these stars shows that [C/Fe] for these stars is about −0.2 while the sample mean is −0.34. The nitrogen ratio [N/Fe] is typically about −0.2 for the high Li stars versus a sample mean of +0.2. It appears that these stars are not processed giants and the high Li abundances reflect their composition on or near the main sequence.

The above argument does not mean there are no super-Li stars in the sample. In fact the well-known super-Li star HD 174104 (Luck 1982) is included and in Figure 11 is the high Li representative at $T = 5854$ K and Li = 3.2 dex. The interpretation of the higher-temperature Li data is that most of the observable Li abundances are associated with stars near the main sequence with those stars having masses around 1.7 $M_\odot$ range. Given the evolutionary timescales, it is likely that most F bright giants are this type of object. F supergiants in the 6000–7000 K range most likely are 5 solar masses and up and are represented in Figure 11 by the Li upper limits. This interpretation is based on the extent of the blue loops in core helium burning (see Iben 1966a, 1966b, 1966c; Schaller et al. 1992; Girardi et al. 2000 for examples). The caveat associated with this interpretation is that CN processed stars in this temperature range exist at all masses (Luck & Lambert 1981, 1985, 1992, 2011). However, they do not show high lithium abundances except in a small number of cases and in very specific areas of the H-R diagram (Reddy & Lambert 2005).

Lithium has been sought in Cepheids in a number of analyses (see, for example, Kovtyukh et al. 2005; Luck & Lambert 2011). This work considers about 45 Cepheids none of which has observable lithium. The upper limit on their lithium content is about 1.8 dex, which is consistent with standard evolutionary theory assuming an initial lithium content of 3.0 dex. Kovtyukh et al. claim to detect lithium in two Cepheids, RX Aur and YZ Aur, at a lithium abundance of about 1.8 dex. Luck & Lambert also investigated these two stars but determined upper limits on the lithium content of 1.9 and 1.2 dex, respectively. The only unequivocal detection of lithium in a Cepheid is for V 1033 Cyg for which Luck & Lambert determined an abundance of 3.2 dex. To reiterate, most intermediate-mass supergiants show upper limits on lithium abundances that are consistent with dilution by first dredge-up standard evolution acting upon a lithium content of 3.0 dex or less. The "less" possibility exists as the amount of lithium remaining in the precursor is strongly dependent on the degree of mass loss prior to the first dredge-up.

4.3.2. CNO

The determination of CNO abundances in luminous stars perhaps starts with the Luck (1978) study of 19 FGK supergiants. The expectation at that time, as is it is now, is that the first dredge-up modifies the surface abundances by enhancing the nitrogen content at the expense of carbon, but leaves the abundance of oxygen intact. For the mass range of interest, the theoretical predictions were initially performed by Iben (1965, 1966a, 1966b, 1966c, 1967), and work up to the present time has borne out those early calculations (for example, Schaller et al. 1992; Girardi et al. 2000). The CN modifications predicted by theoretical models are corroborated by the abundance analyses (for example: Luck 1978; Luck & Lambert 1981, 1985, 1992, 2011; Luck & Heiter 2007), but an unexpected result was that the evolved supergiants showed an unexpected deficiency of oxygen relative to the solar value. This problem has to a large extent gone away with modern determinations of the solar oxygen abundance (see Asplund et al. 2009 for a discussion) yielding a lower solar

Table 7
Mean CNO Data

	Raw			Rejection 1			Rejection 2		
	Mean	σ	N	Mean	σ	N	Mean	σ	N
[Fe/H]	0.042	0.207	457	0.059	0.144	445	0.062	0.115	414
C	8.142	0.469	454	8.163	0.192	449	8.160	0.145	424
N	8.184	0.780	145	8.241	0.375	144	8.222	0.299	136
O	8.675	0.452	457	8.693	0.160	452	8.695	0.120	426
[C/H]	−0.290	0.271	454	−0.283	0.162	439	−0.291	0.135	413
[N/H]	0.249	0.374	145	0.230	0.298	137	0.235	0.251	128
[O/H]	0.004	0.196	457	0.006	0.132	440	0.004	0.109	413
[C/Fe]	−0.334	0.241	454	−0.342	0.159	437	−0.342	0.136	416
[N/Fe]	0.210	0.421	145	0.191	0.307	135	0.167	0.262	127
[O/Fe]	−0.038	0.204	457	−0.052	0.136	433	−0.051	0.114	407
CN	8.475	0.754	145	8.534	0.257	144	8.520	0.189	136
CNO	8.867	0.763	145	8.929	0.180	144	8.917	0.137	137
[C+N/H]	−0.044	0.257	145	−0.059	0.189	137	−0.076	0.157	128
[C+N+O/H]	−0.010	0.179	145	−0.022	0.136	138	−0.028	0.120	132
[CN/Fe]	−0.084	0.311	145	−0.106	0.206	136	−0.119	0.161	125
[CNO/Fe]	−0.050	0.247	145	−0.062	0.167	138	−0.068	0.137	130
C/O	0.335	0.456	454	0.307	0.119	450	0.289	0.077	420

oxygen content more in accord with the value found in young evolved stars such as FGK supergiants. The problem currently might be said to be why should one expect the FGK supergiants to have the same oxygen abundance as the Sun, a much older star that likely migrated to this region of the Milky Way?

The CNO data for this sample indicate that these stars have, on average, undergone standard CN processing and are post-first giant branch objects. Table 7 gives the mean ratios for CNO for the total MARCS determined sample along with the result of applying two 2σ cuts. The pruning eliminates pathological objects such as R CrB. The major effect of trimming the sample is that the standard deviations decrease. Since there is a range of [Fe/H] in the sample, the most relevant abundance ratios for discussion are those with respect to iron. This sample is carbon deficient relative to solar C/Fe by about 0.3 dex, enhanced in nitrogen by about +0.2 dex relative to solar N/Fe, and neutral in oxygen. The mean C/O ratio is about 0.3 versus a solar value of about 0.6. As expected, the *mean* abundances and abundance ratios are consistent with standard evolution of stars more massive than about two solar masses.

Since there exists a wide range in [Fe/H] in the sample, it is of interest to look for trends versus [Fe/H] itself. Figure 12 shows [O/Fe] and [C/Fe] versus [Fe/H], and the trends are very familiar. There is a definite dependence of [O/Fe] and [C/Fe] on [Fe/H]—both increase with decreasing [Fe/H] much as seen in dwarfs and giants (Luck & Heiter 2006, 2007). This is would not be expected in a sample consisting only of young luminous stars. However, as discussed previously, a sample of intrinsically bright stars chosen by spectral type and luminosity class cannot exclude a wide variety of stars that have different masses and evolutionary status. Figure 12 emphasizes that conclusion. The stars in the ensemble clustered about [Fe/H] of +0.1 (see Figure 12(b)) are the stars that should represent the sample from which one could derive the galactic abundance gradient and evolutionary information about intermediate-mass stars. However, even in this group there is strong evidence for a link between [Fe/H] and carbon and oxygen. This is disconcerting as it muddies the interpretation of abundance gradients and suggests that one has to take into account more age and evolution related issues than has been done to date.

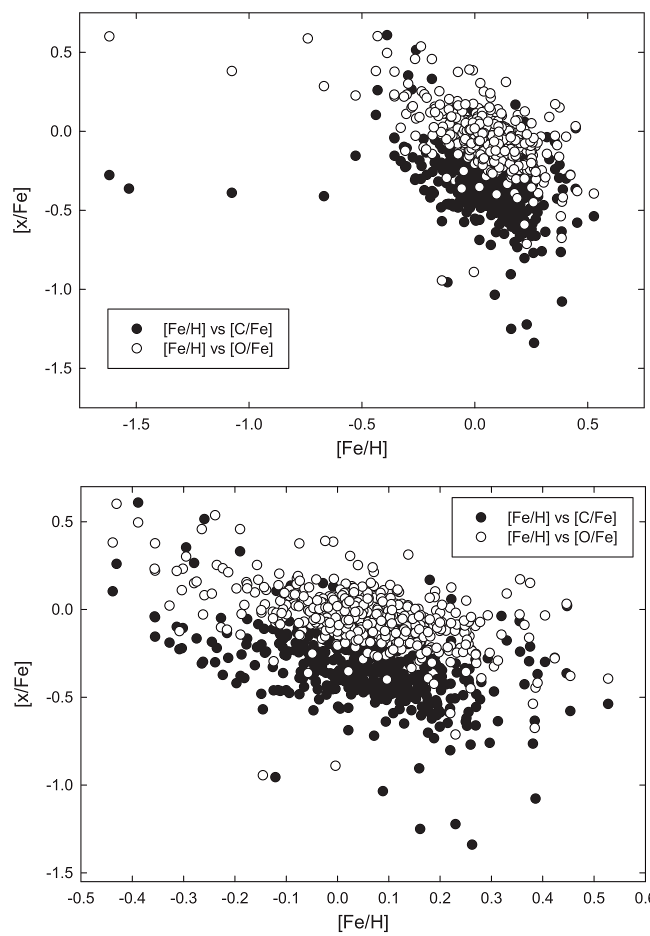

Figure 12. Upper panel: [C/Fe] and [O/Fe] vs. [Fe/H] for the sample using the MARCS abundance determinations. R CrB is the only star not shown. Lower panel: The same data as the upper panel but limited in [Fe/H]. The dependence of [C/Fe] and [O/Fe] on [Fe/H] is clearly seen.

5. CONCLUSIONS

Abundances have been determined for 451 stars, most of which are either supergiants or bright giants. The stars, though chosen to hopefully be consistent in type, show a significant range in abundance and evolutionary status. Nevertheless, due to the sample size, it is possible to determine the galactic abundance gradient $d[\mathrm{Fe/H}]/dR_{\mathrm{G}}$. The value found, -0.05 dex kpc^{-1}, is consistent with previous determinations. The determination is not as secure as the value found from pure Cepheid studies, as Cepheids are more secure in distances and evolutionary status.

There are five summary points to be emphasized.

1. Cepheids are still the better way to do the abundance gradient.
2. Li in these stars shows a wide range and coupled with stellar parameters can be used as a diagnostic of evolutionary status.
3. CNO is as expected for standard processing for the bulk of the sample.
4. These stars show [O/Fe] versus [Fe/H] systematics, indicating a wide range of age though all were selected as luminous—$M > 2\,M_{\odot}$—stars. This means that one must be careful when selecting stars for abundance gradient work.
5. *Gaia* will provide better distances. However, this will not solve the mass discrimination problem as the reddenings, and thus the absolute magnitudes, will likely remain problematic.

It is a pleasure to thank Daniel Lalich for his help in measuring the solar equivalent widths. I thank David Lambert for enabling the acquisition of the Hobby–Eberly Telescope (HET) spectra as part of our observing campaign on Cepheid variables. The Resident Astronomers of the HET are thanked for their help in obtaining the HET observations used in this study. The HET is a joint project of the University of Texas at Austin, the Pennsylvania State University, Stanford University, Ludwig-Maximilians-Universitat Munchen, and Georg-August-Universitat Gottingen. The HET is named in honor of its principal benefactors, William P. Hobby and Robert E. Eberly. Partially based on data obtained from the ESO Science Archive Facility under many request numbers. Also based partially on spectral data retrieved from the ELODIE archive at Observatoire de Haute-Provence (OHP).

REFERENCES

Allende Prieto, C., Lambert, D. L., & Asplund, M. 2001, ApJL, 556, L63
Andersen, J., Gustafsson, B., & Lambert, D. L. 1984, A&A, 136, 65
Andrievsky, S. M., Bersier, D., Kovtyukh, V. V., et al. 2002, A&A, 384, 140
Andrievsky, S. M., Lépine, J. R. D., Korotin, S. A., et al. 2013, MNRAS, 428, 3252
Andrievsky, S. M., Luck, R. E., & Korotin, S. A. 2014, MNRAS, 437, 2106
Asplund, M., Grevesse, N., Sauval, A. J., Allende Prieto, C., & Blomme, R. 2005, A&A, 431, 693
Asplund, M., Grevesse, N., Sauval, A. J., Allende Prieto, C., & Kiselman, D. 2004, A&A, 417, 751
Asplund, M., Grevesse, N., Sauval, A. J., & Scott, P. 2009, ARA&A, 47, 481
Barklem, P. S., & Aspelund-Johansson, J. 2005, A&A, 435, 373
Barklem, P. S., Piskunov, N., & O'Mara, B. J. 2000, A&AS, 142, 467
Biémont, E., Hibbert, A., Godefroid, M., & Vaeck, N. 1993, ApJ, 412, 431
Bond, H. E. 1980, ApJS, 44, 517
Castelli, F. 1996, in ASP Conf. Ser. 108, Model Atmospheres and Stellar Spectra, ed. S. J. Adelman, F. Kupka, & W. W. Weiss (San Francisco, CA: ASP), 85
Castelli, F. 1999, A&A, 346, 564
Cescutti, G., Matteucci, F., François, P., & Chiappini, C. 2007, A&A, 462, 943
Danylewych, L. L., & Nicholls, R. W. 1974, RSPSA, 339, 197
Delbouille, L., Roland, G., & Neven, L. 1973, Photometric atlas of the solar spectrum from 3000 to 10000 Å (Liege: Univ. Liège, Institut d'Astrophysique)
di Benedetto, G. P. 1998, A&A, 339, 858
Fry, M. A., & Aller, L. H. 1975, ApJS, 29, 55
Girardi, L., Bressan, A., Bertelli, G., & Chiosi, C. 2000, A&AS, 141, 371
Grevesse, N., Lambert, D. L., Sauval, A. J., et al. 1991, A&A, 242, 488
Grevesse, N., Noels, A., & Sauval, J. 1996, in ASP Conf. Ser. 99, Standard Abundances, ed. S. S. Holt & G. Sonneborn (San Francisco, CA: ASP), 117
Gustafsson, B., Edvardsson, B., Eriksson, K., et al. 2008, A&A, 486, 951
Hakkila, J., Myers, J. M., & Stidham, B. J. 1997, AJ, 114, 2043
Harris, H. C. 1985, AJ, 90, 756
Hekker, S., & Meléndez, J. 2007, A&A, 475, 1003
Hibbert, A., Biémont, E., Godefroid, M., & Vaeck, N. 1993, A&AS, 99, 179
Hoffleit, D., & Jaschek, C. (ed.) 1991, The Bright Star Catalog (5th ed.; New Haven, CT: Yale University Observatory)
Iben, I. 1965, ApJ, 142, 1447
Iben, I. 1966a, ApJ, 143, 483
Iben, I. 1966b, ApJ, 143, 505
Iben, I. 1966c, ApJ, 143, 516
Iben, I. 1967, ApJ, 147, 650
Johansson, S., Litzén, U., Lundberg, H., & Zhang, Z. 2003, ApJL, 584, L107
Kovtyukh, V. V. 2007, MNRAS, 378, 617
Kovtyukh, V. V., & Andrievsky, S. M. 1999, A&A, 351, 597
Kovtyukh, V. V., Chekhonadskikh, F. A., Luck, R. E., et al. 2010, MNRAS, 408, 1568
Kovtyukh, V. V., Soubiran, C., Luck, R. E., et al. 2008, MNRAS, 389, 1336
Kovtyukh, V. V., Wallerstein, G., & Andrievsky, S. M. 2005, PASP, 117, 1182
Kramida, A., Ralchenko, Yu., Reader, J., & NIST ASD Team 2013, NIST Atomic Spectra Database (ver. 5.1; Gaithersburg, MD: National Institute of Standards and Technology), available online at http://physics.nist.gov/asd
Kurucz, R. L. 1992, in IAU Symp. 149, The Stellar Populations of Galaxies, ed. B. Barbuy & A. Renzini (Dordrecht: Kluwer), 225
Kurucz, R. L., Furenlid, I., Brault, J., & Testerman, L. 1984, Solar Flux Atlas from 296 to 1300 nm (Sunspot, NM: National Solar Observatory)
Lambert, D. L., & Reddy, B. E. 2004, MNRAS, 349, 757
Lèbre, A., de Laverny, P., Do Nascimento, J. D., Jr., & de Medeiros, J. R. 2006, A&A, 450, 1173
Luck, R. E. 1975, ApJ, 202, 743
Luck, R. E. 1978, ApJ, 219, 148
Luck, R. E. 1982, PASP, 94, 811
Luck, R. E., Andrievsky, S. M., Fokin, A, & Kovtyukh, V. V. 2008, AJ, 136, 98
Luck, R. E., Andrievsky, S. M., Korotin, S. N., & Kovtyukh, V. V. 2013, AJ, 146, 18
Luck, R. E., Andrievsky, S. M., Kovtyukh, V. V., Gieren, W. P., & Graczyk, D. 2011, AJ, 142, 51
Luck, R. E., & Heiter, U. 2006, AJ, 131, 3069
Luck, R. E., & Heiter, U. 2007, AJ, 133, 2464
Luck, R. E., & Lambert, D. L. 1981, ApJ, 245, 1018
Luck, R. E., & Lambert, D. L. 1985, ApJ, 298, 782
Luck, R. E., & Lambert, D. L. 1992, ApJS, 79, 303
Luck, R. E., & Lambert, D. L. 2011, AJ, 142, 136
Luck, R. E., Lambert, D. L., & Bond, H. E. 1983, PASP, 95, 413
Luck, R. E., & Wepfer, G. G. 1995, AJ, 110, 2425
Lyubimkov, L. S., Lambert, D. L., Rostopchin, S. I., Rachkovskaya, T. M., & Poklad, D. B. 2010, MNRAS, 402, 1369
McCarthy, J. K., Sandiford, B. A., Boyd, D., & Booth, J. M. 1993, PASP, 105, 881
McWilliam, A. 1990, ApJS, 74, 1075
Moultaka, J., Ilovaisky, S. A., Prugniel, P., & Soubiran, C. 2004, PASP, 116, 693
North, P., Berthet, S., & Lanz, T. 1994, A&A, 281, 775
Rao, N. K., Giridhar, S., & Lambert, D. L. 2012, MNRAS, 419, 1254
Reddy, B. E., & Lambert, D. L. 2005, AJ, 129, 2831
Rutten, R. J., & van der Zalm, E. B. J. 1984a, A&AS, 55, 143
Rutten, R. J., & van der Zalm, E. B. J. 1984b, A&AS, 55, 171
Schaller, G., Schaerer, D., Meynet, G., & Maeder, A. 1992, A&AS, 96, 269
Schönrich, R. 2012, MNRAS, 427, 274
Soubiran, C., Le Campion, J.-F., Cayrel de Strobel, G., & Caillo, A. 2010, A&A, 515, A111
Sneden, C. 1973, PhD dissertation, Univ. Texas-Austin
Sziládi, K., Vinkó, J., Poretti, E., Szabados, L., & Kun, M. 2007, A&A, 473, 579
Tull, R. G. 1998, Proc. SPIE, 3355, 387
Unsöld, A. 1938, Physik der sternamospharen, MIT besonderer berucksichtigung der sonne (Berlin: Springer)
van Leeuwen, F. 2007, A&A, 474, 653
Worley, C. C., de Laverny, P., Recio-Blanco, A., et al. 2012, A&A, 542, 48